JACS
JOURNAL OF THE AMERICAN CHEMICAL SOCIETY

Article

Dynamics of Silica-Supported Catalysts Determined by Combining Solid-State NMR Spectroscopy and DFT Calculations

Frédéric Blanc, Jean-Marie Basset, Christophe Copéret, Amritanshu Sinha, Zachary J. Tonzetich, Richard R. Schrock, Xavier Solans-Monfort, Eric Clot, Odile Eisenstein, Anne Lesage, and Lyndon Emsley

J. Am. Chem. Soc., **2008**, 130 (18), 5886-5900 • DOI: 10.1021/ja077749v • Publication Date (Web): 11 April 2008

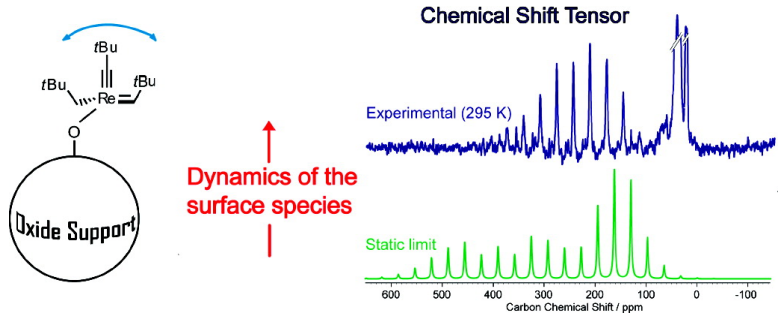

More About This Article

Additional resources and features associated with this article are available within the HTML version:

- Supporting Information
- Access to high resolution figures
- Links to articles and content related to this article
- Copyright permission to reproduce figures and/or text from this article

View the Full Text HTML

Journal of the American Chemical Society is published by the American Chemical Society. 1155 Sixteenth Street N.W., Washington, DC 20036

J|A|C|S
ARTICLES

Published on Web 04/11/2008

Dynamics of Silica-Supported Catalysts Determined by Combining Solid-State NMR Spectroscopy and DFT Calculations

Frédéric Blanc,[†] Jean-Marie Basset,[†] Christophe Copéret,[†] Amritanshu Sinha,[‡] Zachary J. Tonzetich,[‡] Richard R. Schrock,[‡] Xavier Solans-Monfort,[§,||] Eric Clot,[||] Odile Eisenstein,[||] Anne Lesage,[⊥] and Lyndon Emsley*[,⊥]

Laboratoire de Chimie, Catalyse, Polymères et Procédés (UMR 5265), Chimie Organométallique de Surface, ESCPE Lyon, Université de Lyon, 43 Bd du 11 Novembre 1918, F-69616 Villeurbanne, France, Department of Chemistry, Massachusetts Institute of Technology, Cambridge, Massachussets 02139, Departament de Química, Universitat Autònoma de Barcelona, 08193 Bellaterra, Spain, Institut Charles Gerhardt Montpellier (UMR 5253, CNRS, UM2, UM1, ENSCM), Université Montpellier 2, cc 1501, Place E. Bataillon, F-34095 Montpellier, France, and Laboratoire de Chimie (UMR 5182), ENS Lyon, Université de Lyon, 46 Allée d'Italie, F-69364 Lyon, France

Received October 9, 2007; E-mail: lyndon.emsley@ens-lyon.fr

Abstract: The molecular dynamics of a series of organometallic complexes covalently bound to amorphous silica surfaces is determined experimentally using solid-state nuclear magnetic resonance (NMR) spectroscopy and density functional theory calculations (DFT). The determination is carried out for a series of alkylidene-based catalysts having the general formula [(≡SiO)M(ER)(=CH*t*Bu)(R′)] (M = Re, Ta, Mo or W; ER = C*t*Bu, NAr or CH_2*t*Bu; R′ = CH_2*t*Bu, NPh_2, NC_4H_4). Proton−carbon dipolar coupling constants and carbon chemical shift anisotropies (CSA) are determined experimentally by solid-state NMR. Room-temperature molecular dynamics is quantified through order parameters determined from the experimental data. For the chemical shift anisotropy data, we validate and use a method that integrates static values for the CSA obtained computationally by DFT, obviating the need for low-temperature measurements. Comparison of the room-temperature data with the calculations shows that the widths of the calculated static limit dipolar couplings and CSAs are always greater than the experimentally determined values, providing a clear indication of motional averaging on the NMR time scale. Moreover, the dynamics are found to be significantly different within the series of molecular complexes, with order parameters ranging from $<S_z> = 0.5$ for [(≡SiO)Ta(=CH*t*Bu)(CH_2*t*Bu)$_2$] and [(≡SiO)Re(≡C*t*Bu)(=CH*t*Bu)(CH_2*t*Bu)] to $<S_z> = 0.9$ for [(≡SiO)Mo(≡NAr)(=CH*t*Bu)(R′) with R′ = CH_2*t*Bu, NPh_2, NC_4H_4. The data also show that the motion is not isotropic and could be either a jump between two sites or more likely restricted librational motion. The dynamics are discussed in terms of the molecular structure of the surface organometallic complexes, and the orientation of the CSAs tensor at the alkylidene carbon is shown to be directly related to the magnitude of the α-alkylidene CH agostic interation.

1. Introduction

The molecular understanding of heterogeneous catalysis is still one of the key challenges in chemistry. This can be traced in particular to a lack of detailed characterization of the catalytically active sites, which in turn prevents a molecular understanding of activity, reactivity and selectivity versus chemical structure and thereby the rational development of efficient catalysts. One approach to solving this problem is to carry over the advantages of homogeneous catalysts, where structure–activity relationships are well-established (since methods such as X-ray diffraction and nuclear magnetic resonance today allow almost perfect structural characterization). This can be achieved by synthesizing well-defined heterogeneous catalysts either by immobilization of known homogeneous catalysts (supported heterogeneous catalysts) or by covalent grafting of the metal center onto the oxide support (Figure 1).[1,2] Our group[3] and others[4–6] following the second strategy, also called surface organometallic chemistry (SOMC), have synthesized well-defined heterogeneous catalysts that were designed and improved through structure–activity relationships. This approach

[†] ESCPE Lyon, Université de Lyon.
[‡] Massachusetts Institute of Technology.
[§] Universitat Autònoma de Barcelona.
[||] Université Montpellier 2.
[⊥] ENS Lyon, Université de Lyon.

(1) Copéret, C.; Basset, J. M. *Adv. Synth. & Catal.* **2007**, *349*, 78–92.
(2) Copéret, C. *Dalton Trans.* **2007**, *47*, 5498–5504.
(3) Copéret, C.; Chabanas, M.; Petroff Saint-Arroman, R.; Basset, J.-M. *Angew. Chem., Int. Ed.* **2003**, *42*, 156–181.
(4) Ahn, H.; Marks, T. J. *J. Am. Chem. Soc.* **2002**, *124*, 7103–7110.
(5) Fischbach, A.; Klimpel, M. G.; Widenmeyer, M.; Herdtweck, E.; Scherer, W.; Anwander, R. *Angew. Chem., Int. Ed.* **2004**, *43*, 2234–2239.
(6) Weissman, H.; Plunkett, K. N.; Moore, J. S. *Angew. Chem., Int. Ed.* **2006**, *45*, 585–588.

 10.1021/ja077749v CCC: $40.75

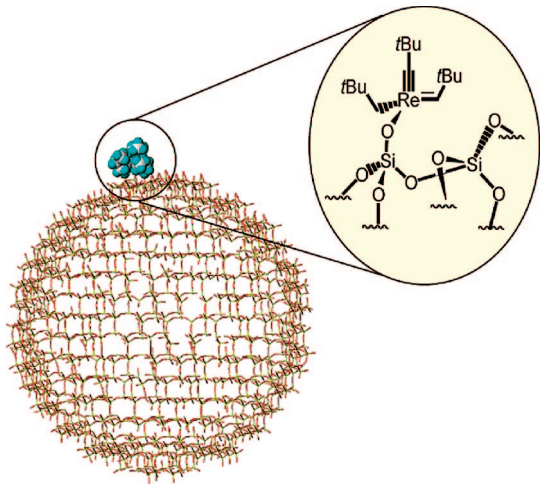

Figure 1. Schematic representation of the systems under investigation here (example of [**ReR**]). The organometallic fragment [Re(≡C*t*Bu)(=CH*t*Bu)(CH_2*t*Bu)] is covalently bounded to the silica through Si−O−Re moiety. Only one surface complex is represented for the sake of simplicity.

offers new possibilities in terms of stability and reactivity in comparison with homogeneous and classical heterogeneous catalysts.[1,7,8] Much of the success of this "single-site" heterogeneous approach is due to the fact that we have progressively been able to adapt characterization techniques from solution or single crystal methods to these surface bound systems.[1,3,9] Notably, we have shown that magic-angle-spinning solid-state NMR spectroscopy can play a role of premier importance in characterizing molecularly these systems.[9–21] Several different methods have been developed to correlate proton spins, such as proton−proton double quantum (DQ)[15] or triple quantum spectroscopy (TQ)[20] or combined rotation and multiple sequence (CRAMPS),[18] to correlate protons with carbon (or nitrogen) spins through heteronuclear correlation (HETCOR) spectroscopy,[11] and to extract structural parameters including scalar $^1J_{CH}$ coupling constants in the solid state on a range of different catalysts.[9,13]

As an example, exhaustive solid-state NMR analysis has been used for the detailed structural characterization of a series of well-defined alkylidene-based complexes bound to silica of the general formula [(≡SiO)M(ER)(=CH*t*Bu)(R′)] (M = Re, ER = C*t*Bu, R′ = CH_2*t*Bu,[12,14] labeled [**ReR**]; M = Ta, ER = R′ = CH_2*t*Bu,[11] labeled [**TaR**]; M = Mo, ER = NAr (Ar = 2,6-*i*$Pr_2C_6H_3$), R′ = CH_2*t*Bu,[18] labeled [**MoR**]; M = W, ER = NAr (Ar = 2,6-*i*$Pr_2C_6H_3$), R′ = CH_2*t*Bu,[22] labeled [**WR**]; M = Mo, ER = NAr, R′ = NPh_2,[23] labeled [**MoNPh$_2$**]; M = Mo, ER = NAr, R′ = Pyrrolyl,[23] labeled [**MoPy**]) (see Chart 1 for molecular structures). These complexes have displayed unsual and very promising catalytic activities for metathesis reactions[16,18,22–25] by comparison with their homogeneous analogues,[26] but there is still a need to understand these systems in fine detail if one want to undertake a more rational improvement of them.

It is today well-known that dynamics play a key role in a large range of chemical systems, from proteins and nucleic acids[27] through supramolecular "machines",[28,29] polymers,[30] inorganic systems,[31] crystalline and disordered solids,[30,32] and molecules trapped in porous materials.[33,34] In each case, NMR has been shown to be univoquably positioned to study molecular dynamics

Recent results, based on calculations of [**ReR**], have shown that the reactivity toward olefins is in part due to the distortion of these catalysts from the original pseudotetrahedral geometry to a distorted trigonal pyramid.[35,36] We have therefore decided to investigate the molecular dynamics in these silica bound materials, where the potential role of dynamics has so far been

(7) Fierro-Gonzalez, J. C.; Kuba, S.; Hao, Y. L.; Gates, B. C. *J. Phys. Chem. B* **2006**, *110*, 13326–13351.
(8) Haw, J. F.; Nicholas, J. B.; Xu, T.; Beck, L. W.; Ferguson, D. B. *Acc. Chem. Res.* **1996**, *29*, 259–267.
(9) Blanc, F.; Copéret, C.; Lesage, A.; Emsley, L. *Chem. Soc. Rev.* **2008**, *37*, 518–526.
(10) Petroff Saint-Arroman, R.; Chabanas, M.; Baudouin, A.; Copéret, C.; Basset, J.-M.; Lesage, A.; Emsley, L. *J. Am. Chem. Soc.* **2001**, *123*, 3820–3821.
(11) Chabanas, M.; Quadrelli, E. A.; Fenet, B.; Copéret, C.; Thivolle-Cazat, J.; Basset, J.-M.; Lesage, A.; Emsley, L. *Angew. Chem., Int. Ed.* **2001**, *40*, 4493–4496.
(12) Chabanas, M.; Baudouin, A.; Copéret, C.; Basset, J.-M *J. Am. Chem. Soc.* **2001**, *123*, 2062–2063.
(13) Lesage, A.; Emsley, L.; Chabanas, M.; Copéret, C.; Basset, J.-M. *Angew. Chem., Int. Ed.* **2002**, *41*, 4535–4538.
(14) Chabanas, M.; Baudouin, A.; Copéret, C.; Basset, J.-M.; Lukens, W.; Lesage, A.; Hediger, S.; Emsley, L. *J. Am. Chem. Soc.* **2003**, *125*, 492–504.
(15) Rataboul, F.; Baudouin, A.; Thieuleux, C.; Veyre, L.; Copéret, C.; Thivolle-Cazat, J.; Basset, J.-M.; Lesage, A.; Emsley, L. *J. Am. Chem. Soc.* **2004**, *126*, 12541–12550.
(16) Le Roux, E.; Chabanas, M.; Baudouin, A.; de Mallmann, A.; Copéret, C.; Quadrelli, E. A.; Thivolle-Cazat, J.; Basset, J.-M.; Lukens, W.; Lesage, A.; Emsley, L.; Sunley, G. J. *J. Am. Chem. Soc.* **2004**, *126*, 13391–13399.
(17) Kervern, G.; Pintacuda, G.; Zhang, Y.; Oldfield, E.; Roukoss, C.; Kuntz, E.; Herdtweck, E.; Basset, J. M.; Cadars, S.; Lesage, A.; Copéret, C.; Emsley, L. *J. Am. Chem. Soc.* **2006**, *128*, 13545–13552.
(18) Blanc, F.; Copéret, C.; Thivolle-Cazat, J.; Basset, J.-M.; Lesage, A.; Emsley, L.; Sinha, A.; Schrock, R. R. *Angew. Chem., Int. Ed.* **2006**, *45*, 1216–1220.
(19) Blanc, F.; Copéret, C.; Thivolle-Cazat, J.; Basset, J.-M.; Lesage, A.; Emsley, L.; Sinha, A.; Schrock, R. R. *Inorg. Chem.* **2006**, *45*, 9587–9592.
(20) Avenier, P.; Lesage, A.; Taoufik, M.; Baudouin, A.; De Mallmann, A.; Fiddy, S.; Vautier, M.; Veyre, L.; Basset, J. M.; Emsley, L.; Quadrelli, E. A. *J. Am. Chem. Soc.* **2007**, *129*, 176–186.
(21) Avenier, P.; Taoufik, M.; Lesage, A.; Baudouin, A.; Solans-Monfort, X.; De Mallmann, A.; Veyre, L.; Basset, J. M.; Eisenstein, O.; Emsley, L.; Quadrelli, E. A. *Science* **2007**, *317*, 1056.
(22) Rhers, B.; Salameh, A.; Baudouin, A.; Quadrelli, E. A.; Taoufik, M.; Copéret, C.; Lefebvre, F.; Basset, J.-M.; Solans-Monfort, X.; Eisenstein, O.; Lukens, W.; Lopez, L. P. H.; Sinha, A.; Schrock, R. R. *Organometallics* **2006**, *25*, 3554–3557.
(23) Blanc, F.; Thivolle-Cazat, J.; Basset, J.-M.; Copéret, C.; Hock, A. S.; Tonzetich, Z. J.; Sinha, A.; Schrock, R. R. *J. Am. Chem. Soc.* **2007**, *129*, 1044–1045.
(24) Chabanas, M.; Copéret, C.; Basset, J.-M. *Chem. Eur. J.* **2003**, *9*, 971–975.
(25) Blanc, F.; Copéret, C.; Thivolle-Cazat, J.; Basset, J.-M. *Angew. Chem., Int. Ed.* **2006**, *45*, 6201–6203.
(26) Schrock, R. R. *Angew. Chem., Int. Ed.* **2006**, *45*, 3748–3759.
(27) Mittermaier, A.; Kay, L. E. *Science* **2006**, *312*, 224–228.
(28) Balzani, V.; Gomez-Lopez, M.; Stoddart, J. F. *Acc. Chem. Res.* **1998**, *31*, 405–414.
(29) Sauvage, J. P. *Acc. Chem. Res.* **1998**, *31*, 611–619.
(30) Schmidt-Rohr, K.; Spiess, H. W. *Multidimensional Solid-state NMR and Polymers*; Academic Press: London, 1994.
(31) Abel, E. W.; Coston, T. P. J.; Orrell, K. G.; Sik, V.; Stephenson, D. *J. Magn. Reson.* **1986**, *70*, 34–53.
(32) Steigel, A.; Spiess, H. W. *NMR Basic Principles and Progress*; Springer-Verlag: Berlin, Heidelberg, New York, 1978.
(33) Pizzanelli, S.; Kababya, S.; Frydman, V.; Landau, M.; Vega, S. *J. Phys. Chem. B* **2005**, *109*, 8029–8039.
(34) Buntkowsky, G.; Breitzke, H.; Adamezyk, A.; Roelofs, F.; Emmler, T.; Gedat, E.; Grunberg, B.; Xu, Y.; Limbach, H. H.; Shenderovich, J.; Vyalikh, A.; Findenegg, G. *Phys. Chem. Chem. Phys.* **2007**, *9*, 4843–4853.
(35) Solans-Monfort, X.; Clot, E.; Copéret, C.; Eisenstein, O. *J. Am. Chem. Soc.* **2005**, *127*, 14015–14025.
(36) Poater, A.; Solans-Monfort, X.; Clot, E.; Copéret, C.; Eisenstein, O. *J. Am. Chem. Soc.* **2007**, *129*, 8207–8216.

Chart 1. Shematic Representation of All Considered Surface Organometallic Complexes Studied and Their Fragments for DFT Calculations

Experimental	Fragments for DFT calculations		
	Periodic	Cluster_1	Cluster_2
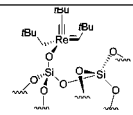	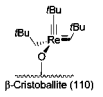	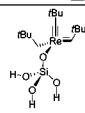	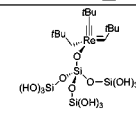
***syn*-[ReR]**	***syn*-ReR-C**	***syn*-ReR-C1**	***syn*-ReR-C2**
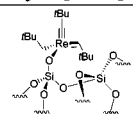	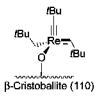	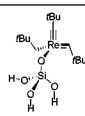	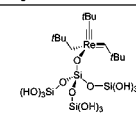
***anti*-[ReR]**	***anti*-ReR-C**	***anti*-ReR-C1**	***anti*-ReR-C2**
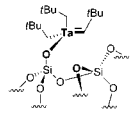	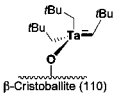	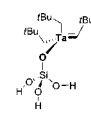	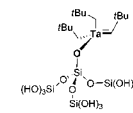
[TaR]	**TaR-C**	**TaR-C1**	**TaR-C2**
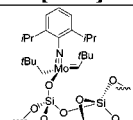	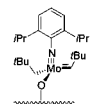	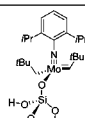	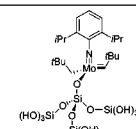
***syn*-[MoR]**	***syn*-MoR-C**	***syn*-MoR-C1**	***syn*-MoR-C2**
	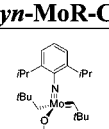	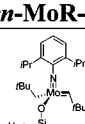	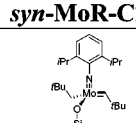
***anti*-[MoR]**	***anti*-MoR-C**	***anti*-MoR-C1**	***anti*-MoR-C2**
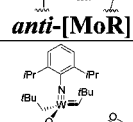	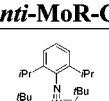	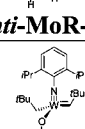	
***syn*-[WR]**	***syn*-WR-C**	***syn*-WR-C1**	***syn*-WR-C2**
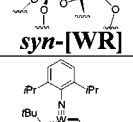		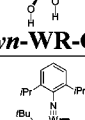	
***anti*-[WR]**	***anti*-WR-C**	***anti*-WR-C1**	***anti*-WR-C2**
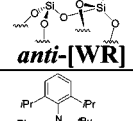		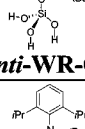	
***syn*-[MoNPh$_2$]**	***syn*-MoNPh$_2$-C**	***syn*-MoNPh$_2$-C1**	***syn*-MoNPh$_2$-C2**
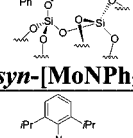	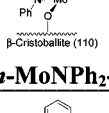	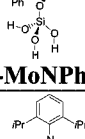	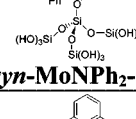
***anti*-[MoNPh$_2$]**	***anti*-MoNPh$_2$-C**	***anti*-MoNPh$_2$-C1**	***anti*-MoNPh$_2$-C2**
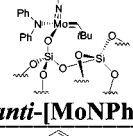	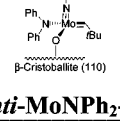	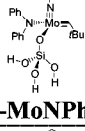	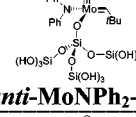
***syn*-[MoPy]**	***syn*-MoPy-C**	***syn*-MoPy-C1**	***syn*-MoPy-C2**
***anti*-[MoPy]**	***anti*-MoPy-C**	***anti*-MoPy-C1**	***anti*-MoPy-C2**

neglected through solid-state NMR spectroscopy.[30,32] The systems under consideration here (Chart 1 and Figure 1) are significantly different from the one previously mentioned above as the organometallic complexes are covalently bound to silica via Si−O−M bonds and not adsorbed on the oxide surface. Moreover, EXAFS has shown that there is possibly an interaction of the metal with the surface through a siloxane bridge Si−O−Si.[14] Among the well-known NMR dynamics probes, *we have chosen to use both the dipolar tensors, i.e., residual dipolar couplings (RDC), and the chemical shift tensors, i.e., chemical shift anisotropy (CSA), to provide information about the dynamics*.

One-dimensional solid-state NMR experiments under magic angle spinning (MAS) have classically been used to measure fast-limit dynamics by measuring the chemical shielding tensors.[37,38] The information obtained is a time-averaged tensor, and the quantitative analysis of the motion *requires knowledge of the static limit tensor*.[38] While this static limit dipolar coupling constant b_{CH} is easily obtained from the bond distance r_{CH} using eq 1 (for a CH for example),

$$b_{CH} = -\frac{\mu_0 \hbar^2 \gamma_c \gamma_H}{4\pi r_{CH}^3} \quad (1)$$

the static limit chemical shift tensor has been obtained previously by observing a spectrum at sufficiently low temperatures in the absence of motion. This is a strong constraint on the applicability of NMR dynamics studies, both in terms of chemical (time scale) and instrumental factors. Notably it is not easily practical for the systems of interest here (Chart 1) for the following reasons: the frozen regime is expected at very low temperatures (vide infra) and the weak NMR sensitivity of silica-supported samples[3] requires long experiments for which low temperatures are difficult to obtain. Specifically, in these systems the concentration is only about 0.5 molecule/nm^2 of surface, which translates to 0.2 mmol/g (this is currently about an order of magnitude less than what would be typically considered required for low-temperature studies to be viable). Moreover, we also want to validate an approach which uses DFT as a tool to obtain the static limit tensors (see below). We note that as a consequence, only very few pioneering studies of dynamics obtained by CSA have already been reported for molecules chemically bonded to surfaces including organic[39–41] or organometallic[42–44] fragments bound to silica.

The tremendous recent progress made by DFT-based methods for calculation of NMR data,[45] including chemical shift, even in transition-metal-containing inorganic systems,[46] allows the computation of reliable NMR data.[47–49] The approach usually only determines the NMR values for the global minimum of the potential energy surface, that is, without taking into account the dynamic motion of the system. Therefore, the computed chemical shift tensors correspond to a static limit chemical shift tensor. That is, *DFT calculations can be used to establish the static limit chemical shift tensor with reasonable accuracy*, accuracy which can be evaluated by the calculated isotropic chemical shift δ_{iso}^{calc}. This approach has recently been used in structural biology to quantify dynamics of ergosterol's in membranes.[50]

In this article, we first obtain dynamics parameters of various catalysts (Chart 1), by measuring the $^{13}C-^{1}H$ dipolar tensors using dipolar-shift[51] (dipshift) correlation by solid-state NMR. We then compare our RDC dynamics data to an approach using ^{13}C chemical shift tensors combining NMR measurements with DFT calculations. Both qualitative and quantitative analysis of the motion are performed through fitting of spectral line shapes and determination of motional order parameters.[38,52–55] We find remarkable differences in the amplitude of the measured molecular dynamics from one complex to another, as a function of the metal and the ligand. We also find that the motion is not a simple free rotation about the M−O and Si−O bonds and speculate on the possibility of a dynamics−function relationship in those systems. Finally, we find a relation between the orientation of the chemical shift tensor and the agosticity of the CH^{α} bond.

2. Materials and Methods

2.1. Sample Preparations. All the covalently silica bound organometallic complexes were prepared, including the synthesis of their ^{13}C-labeled ligands, as previously described: [(≡SiO)Re(≡*C*t*Bu)(=*CH*t*Bu)(*CH$_2$*t*Bu)][12,14] [**ReR**], [(≡SiO)Ta(=*CH*t*Bu)(*CH$_2$*t*Bu)$_2$][11,16,56] [**TaR**], *syn*-[(≡SiO)Mo(≡NAr)(=*CH*t*Bu)(*CH$_2$*t*Bu)][18] [**MoR**], *syn*-[(≡SiO)W(≡NAr)(=*CH*t*Bu)(*CH$_2$*t*Bu)][22] [**WR**] *syn*-[(≡SiO)Mo(≡NAr)(=*CH*t*Bu)(NPh$_2$)][23] [**MoNPh$_2$**] and *syn*-[(≡SiO)Mo(≡NAr)(=*CH*t*Bu)(NC$_4$H$_4$)][23] [**MoPy**]. Natural abundance L-alanine was purchased from Sigma Aldrich and used without further recrystallization.

2.2. Solid-State NMR Spectroscopy. All solid-state NMR spectra were recorded on a Bruker Avance 500 wide-bore NMR spectrometer operating at ^{1}H and ^{13}C Larmor frequencies of 500.14 and 125.76 MHz, respectively.[57] A double resonance 4-mm cross-polarization (CP) MAS probe was used for all experiments. Unless otherwise specified, the samples (around 30 mg) were packed in a rotor in a glovebox under an inert atmosphere and tightly closed. A ^{1}H MAS NMR spectra was recorded at the end of each acquisition to ensure stability of the complexes. Unless otherwise specified, the temperature of the sample was regulated at 295 ± 1 K. Carbon chemical shifts are referenced to liquid TMS at 0 ppm.

(37) Sparks, S. W.; Cole, H. B. R.; Torchia, D. A.; Young, P. E. *Chem. Scr.* **1989**, *29A*, 31–38.
(38) Cole, H. B. R.; Torchia, D. A. *Chem. Phys.* **1991**, *158*, 271–281.
(39) Slotfeldtellingsen, D.; Resing, H. A. *J. Phys. Chem.* **1980**, *84*, 2204–2209.
(40) Koller, H.; Wolker, A.; Villaescusa, L. A.; Diaz-Cabanas, M. J.; Valencia, S.; Camblor, M. A. *J. Am. Chem. Soc.* **1999**, *121*, 3368–3376.
(41) Saalwachter, K.; Krause, M.; Gronski, W. *Chem. Mater.* **2004**, *16*, 4071–4079.
(42) Walter, T. H.; Frauenhoff, G. R.; Shapley, J. R.; Oldfield, E. *Inorg. Chem.* **1991**, *30*, 4732–4739.
(43) Engelke, F.; Bhatia, S.; King, T. S.; Pruski, M. *Phys. Rev. B* **1994**, *49*, 2730–2738.
(44) Moroz, B. L.; Moudrakovski, I. L.; Likholobov, V. A. *J. Mol. Catal.* **1996**, *112*, 217–233.
(45) Kaupp, M.; Bühl, M.; Malkin, V. G. *Calculation of NMR and EPR Parameters*; Wiley-VCH: Weinheim, 2004.
(46) Ziegler, T.; Autschbach, J. *Chem. Rev.* **2005**, *105*, 2695–2722.
(47) Davidson, E. R *Chem. Rev* **2000**, *100*, 351–352, and all articles in this issue.
(48) Koch, W.; Holthausen, M. C. A. *Chemist's Guide to Density Functional Theory*; Wiley-VCH: Chichester, 2000.
(49) Harris, R. K. *Solid State Sci.* **2004**, *6*, 1025–1037.
(50) Soubias, O.; Jolibois, F.; Massou, S.; Milon, A.; Reat, V. *Biophys. J.* **2005**, *89*, 1120–1131.
(51) Munowitz, M. G.; Griffin, R. G.; Bodenhausen, G.; Huang, T. H. *J. Am. Chem. Soc.* **1981**, *103*, 2529–2533.
(52) Lipari, G.; Szabo, A. *J. Am. Chem. Soc.* **1982**, *104*, 4546–4559.
(53) Lipari, G.; Szabo, A. *J. Am. Chem. Soc.* **1982**, *104*, 4559–4570.
(54) Torchia, D. A. *J. Magn. Reson.* **1985**, *64*, 135–141.
(55) Lorieau, J. L.; McDermott, A. E. *J. Am. Chem. Soc.* **2006**, *128*, 11505–11512.
(56) See ref 4 for a detailed description of its synthesis.
(57) http://www.ens-lyon.fr/CHIMIE/Fr/Groupes/NMR/Pages/home.html.

The proton−carbon heteronuclear dipolar coupling constants were determined with the dipshift method[51] using DUMBO-1 as the homonuclear decoupling sequence.[58,59] The pulse sequence, available from our Web site[57] or upon request from the authors, starts with a cross polarization step to transfer the proton magnetization to the carbon nuclei (Figure S1, Supporting Information). During the evolution period t_1, which is inserted in a constant-time delay of two rotor periods τ_R, the proton–proton dipolar couplings are removed by DUMBO-1 homonuclear decoupling. The synchronized 180° carbon pulse applied in the middle of the 2 τ_R period refocuses the chemical shift. The chemical shift anisotropy, is averaged out over the two rotor periods. As a result, during t_1, the carbon magnetization is only modulated by the heteronuclear dipolar couplings and yields a spectrum that allows the determination of b_{CH}. All the dipolar spectral information in ω_1 is contained in the t_1 signal sampled over a simple rotor period, which allows a shortened version of the original dipshift experiment to be recorded.[60–62] The dipolar spectra were constructed by a Fourier transform of the time signal obtained (i) by summing the t_1 free induction decays of the isotropic chemical shift and the spinning side bands in ω_2 (recorded over one rotor period) and (ii) by concatenating the resulting time signal over several rotor periods. The intensity of each concatenated signal was weighted in order to take into account signal attenuation due to transverse dephasing. An average of 10 time signals was typically concatenated to reach zero intensity. No apodization was applied before Fourier Transform.

The experimental (scaled) dipolar constants $<b_{CH}^{exp}>$ were obtained by fitting the resulting dipolar spectra using the SIMPSON[63] software. From the fitted values, 1D dipolar spectra were calculated (spectra in red in Figures 2, 3, and S2−S6) with SIMPSON[63] using standard numerical techniques[64] (see above). Unless otherwise specified, all dipolar coupling constants reported here are corrected for the scaling factor of the DUMBO-1 decoupling sequence. The estimated errors associated with the measurement of the heteronuclear dipolar couplings were calculated by varying randomly the fitted values around the best fit values (with a standard deviation given by the spectral noise level) and fitting the obtained dipolar spectra. The dipolar order parameter $<S_z>^{RDC}$ was determined as the ratio of the experimentally determined $^1H-^{13}C$ dipolar coupling constant $<b_{CH}^{exp}>$ to the value of the static limit dipolar coupling constant b_{CH}^{calc} calculated from the carbon−proton bond length of the optimized geometry (see below and Table S1).[65] The bond length used for L-alanine was obtained from DFT calculations in the literature.[66]

The experimental CSA parameters were extracted from 1D carbon-13 spectra recorded at low MAS frequencies. The experimental values of the principal elements of the CSA tensors were obtained by fitting the spinning sideband manifolds using a home written C program.[67,68] From the resulting values, carbon-13 spectra were then calculated (spectra in red in Figures 4–7 and S7−S13) with the SIMPSON[63] software using standard numerical techniques.[64] The powder averaging was performed with the γ compute method, 4180 molecular orientations $\{\alpha_{MR}, \beta_{MR}\}$ using the ZCW algorithm[69] and stepping the Euler angle γ_{MR} over 45 discrete

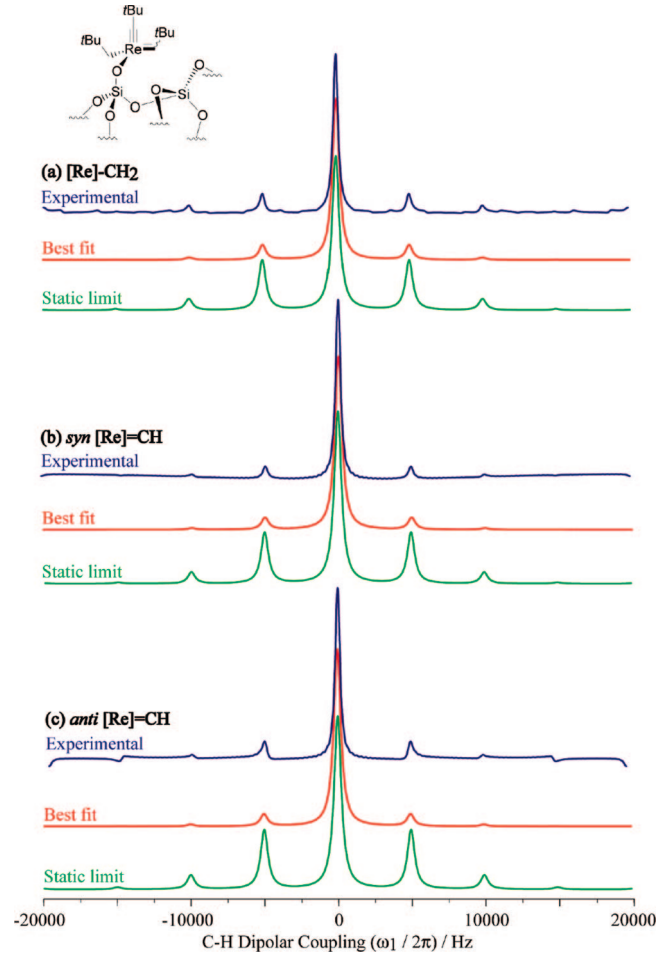

Figure 2. Carbon proton dipolar spectra of [(≡SiO)Re(≡C*t*Bu)(═CH*t*Bu)(CH_2*t*Bu)] ([**ReR**]) under MAS at 5 kHz. Blue lines are the experimental data. Red lines are SIMPSON[63] best-fit simulated spectra. Green lines are SIMPSON[63] simulation of the models ***syn*-ReR-C**. (a) Methylene resonance (δ_{iso}^{exp} = 44 ppm) fitted to a dipolar coupling of $<b_{CH}^{exp}>$ = − 12.5 ± 3.0 kHz. (b) *syn*-Alkylidene resonance (δ_{iso}^{exp} = 247 ppm) fitted to a dipolar coupling of $<b_{CH}^{exp}>$ = − 11.0 ± 4.1 kHz. (c) *anti*-Alkylidene resonance (δ_{iso}^{exp} = 257 ppm) fitted to a dipolar coupling of $<b_{CH}^{exp}>$ = −10.9 ± 4.9 kHz. A total of 21 t_1 increments of 10 μs with 3072 scans each were collected. The recycle delay was set to 2 s. For the CP step, a ramped RF field of 1 ms centered at 60 kHz was applied on protons, while the carbon RF field was matched to obtain optimal signal. The proton and carbon RF fields were set to 100 kHz for pulses, DUMBO-1 homonuclear decoupling,[58,59] and SPINAL-64 heteronuclear decoupling.[115] The total experimental acquisition time was 36 h. An exponential line broadening of 80 Hz was applied before Fourier transform. The DUMBO-1 homonuclear decoupling scheme was programmed as a shape file containing 512 basic cycles, each of them digitized into 64 steps of 500 ns. An experimental scaling constant λ_{exp} of 0.45 was calculated at a MAS frequency of 2.5–5 kHz as the ratio of the experimental heteronuclear $^1J_{CH}$ coupling constant of the CH_3 moiety in alanine and the unscaled 127 Hz value measured in the liquid state NMR spectrum.

(58) Sakellariou, D.; Lesage, A.; Hodgkinson, P.; Emsley, L. *Chem. Phys. Lett.* **2000**, *319*, 253–260.
(59) Lesage, A.; Sakellariou, D.; Hediger, S.; Elena, B.; Charmont, P.; Steuernagel, S.; Emsley, L. *J. Magn. Reson.* **2003**, *163*, 105–113.
(60) Schaefer, J.; McKay, R. A.; Stejskal, E. O. *J. Magn. Reson.* **1983**, *52*, 123–129.
(61) Schaefer, J.; Stejskal, E. O.; McKay, R. A.; Dixon, W. T. *Macromolecules* **1984**, *17*, 1479–1489.
(62) Schaefer, J.; Stejskal, E. O.; Perchak, D.; Skolnick, J.; Yaris, R. *Macromolecules* **1985**, *18*, 368–373.
(63) Bak, M.; Rasmussen, J. T.; Nielsen, N. C. *J. Magn. Reson.* **2000**, *147*, 296–330.
(64) Hodgkinson, P.; Emsley, L. *Prog. Nucl. Magn. Reson. Spectrosc.* **2000**, *36*, 201–239.
(65) Note that we could have also used an average static limit dipolar coupling constant of –22.5 kHz based simply on a CH bond length of 1.102 Å which is not significantly different from the DFT values (Table S1) and which is well within the error of the data in any experiments reported here.
(66) Kumar, S.; Kumar Rai, A.; Rai, S. B.; Rai, D. K.; Singh, A. N.; Singh, V. B. *J. Mol. Struct.* **2006**, *791*, 23–29.
(67) Herzfeld, J.; Berger, A. E. *J. Chem. Phys.* **1980**, *73*, 6021–6030.
(68) Herzfeld, J.; Chen, X. Sideband Analysis in Magic Angle Spinning NMR of Solids. In *Encyclopedia of Nuclear Magnetic Resonance*; Grant, D. M., Harris, R. K., Eds.; Wiley: Chichester, 1996; Vol. 4, pp 4362–4369.
(69) Koons, J. M.; Highes, E.; Cho, H. M.; Ellis, P. D. *J. Magn. Reson. A* **1995**, *114*, 12–23.

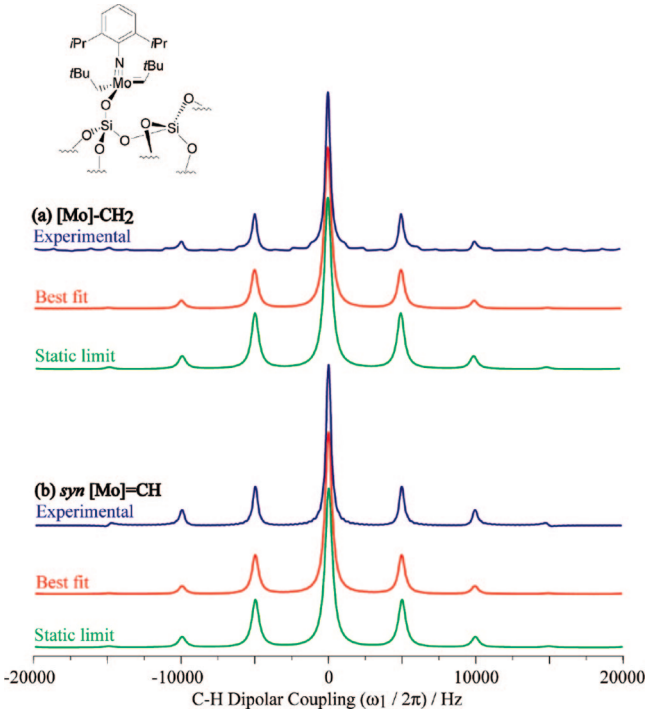

Figure 3. Carbon proton dipolar spectra of *syn*-[(≡SiO)Mo(≡NAr)(=CH*t*Bu)(CH_2*t*Bu)] ([**MoR**]) under MAS at 5 kHz. Blue lines are the experimental dipolar projection obtained by summing up all cross-sections in the F_1 domain. Red lines are SIMPSON[63] best-fit simulated spectra. Green lines are SIMPSON[63] simulation of the models ***syn*-MoR-C**. (a) Methylene resonance ($\delta_{iso}^{exp} = 56$ ppm) fitted to a dipolar coupling of $<b_{CH}^{exp}> = -19.5 \pm 1.6$ kHz. (b) Alkylidene resonance ($\delta_{iso}^{exp} = 279$ ppm) fitted to a proton to a dipolar coupling of $<b_{CH}^{exp}> = -19.7 \pm 2.7$ kHz. All the experimental details are as described previously in Figure 2.

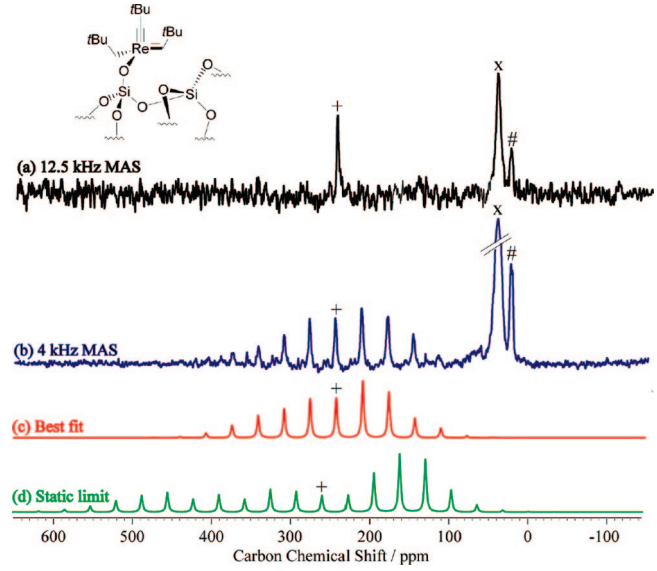

Figure 4. NMR spectra of *syn*-[(≡SiO)Re(≡*C*t*Bu)(=*CH*t*Bu)(*CH_2*t*Bu)] ([**ReR**]). (a) Black: ^{13}C CP MAS spectrum recorded at $\nu_R = 12.5$ kHz with 15360 transients. The contact time for CP was set to 1 ms. (b) Blue: ^{13}C CP MAS spectrum recorded at $\nu_R = 4$ kHz with 18000 transients. The contact time for CP was 1 ms. (c) Red: best-fit simulated spinning side bands of the alkylidene carbon *syn*-[Re](=***C***H*t*Bu) ($\delta_{iso}^{exp} = 247$ ppm, $<\delta_{aniso}^{exp}> = 125 \pm 6$ ppm, $<\eta^{exp}> = 0.87 \pm 0.04$). (d) Green: simulation of the spinning side bands of the alkylidene carbon of the models ***syn*-ReR-C1** ($\delta_{iso}^{calc} = 259$ ppm, $\sigma_{aniso}^{calc} = 306$ ppm, $\eta^{calc} = 0.08$). Labels +, ×, and # show the isotropic resonances of the alkylidene *syn*-[Re]=***C***H, methylene [Re]=***C***H_2, and the ***C***H_3 (not ^{13}C-labeled) resonance, respectively. A ramped CP at a RF field centered at 60 kHz was applied on protons, while the carbon RF field was matched to obtain optimal signal. The recycle delay was set to 2 s. Heteronuclear decoupling in t_2 was performed with SPINAL-64[115] at a proton radio frequency (RF) field of 83 kHz. An exponential line broadening of 80 Hz was applied before Fourier transform.

values. Transverse relaxation was artificially taken into account by applying a Lorentzian line broadening of 200–600 Hz to the calculated free induction decay. Isotropic δ_{iso}^{exp}, anisotropic chemical shift $<\delta_{aniso}^{exp}>$ and asymmetry parameters $<\eta^{exp}>$ are obtained from the principal elements of the CSA tensors using the Haeberlen convention[70] as mentioned in the text. The order parameter $<S_z>^{CSA}$ was measured as the ratio of the experimental determined chemical shift anisotropy $<\delta_{aniso}^{exp}>$ to the value of the static limit anisotropy δ_{aniso}^{calc}, the latest being determined from DFT calculations of the shielding tensor (see below).

2.3. Computational Details. Following our previously validated method[71] (for more details and discussion of the optimized structures, Figures S16 and S17, and Table S1, including the density of states (DOS) projected on the valence d orbitals of the metal, Figure S18, see Supporting Information), geometry optimizations have been performed using periodic DFT calculations within the projector augmented-wave (PAW) formalism[72,73] as implemented in the VASP package.[74,75] Discussion of the calculated data (see Supporting Information) confirms that the siloxy functional group of a silica surface acts only as a large X type ligand and that the system is molecular in nature.[71] The exchange-correlation energy and potential are described by the PBE functional.[76] We have used Monkhorst−Pack[77] sampling of Brillouin zone with a (2,2,1) mesh. The plane wave cutoff has been fixed to 400 eV. The convergence with the number of *k*-points and with the basis set has been tested in our work[71] on the structure of [(≡SiO)Re(≡C*t*Bu)(=CH*t*Bu)-(CH_2*t*Bu)]-supported catalyst and no significant difference is observed for larger *k*-points and higher cutoff. Geometries are given in Figures S16 and S17 and bond distances and angles are summarized in Table S1.

Because VASP does not implement chemical shift calculations, NMR data have been calculated with two finite cluster models that include the full set of ligands, the stereochemistry (*syn* and *anti*) of the metal–carbon double bond, if needed, and one or two shells of OSi units, [M(ER)(=CH*t*Bu)(R′)($OSi(OH)_3$)] (cluster_1) and [M(ER)(=CH*t*Bu)(R′)($OSi(OSi(OH)_3)_3$] (cluster_2) (M = Re, ER = C*t*Bu, R′ = CH_2*t*Bu; M = Ta, ER = R′ = CH_2*t*Bu; M = Mo and W, ER = NAr, R = CH_2*t*Bu; M = Mo, ER = NAr, R′ = NPh_2; M = Mo, ER = NAr, R′ = pyrrolyl noted Py) (Ar = 2,6-*i*$Pr_2C_6H_3$). Those models where labeled ***p*-MR′-C*x*** where *x* is 1 or 2 depending on the cluster size. The effect of the cluster size has been tested previously for calculated $^1J_{CH}$ coupling constants. For all models the calculated results were reasonably similar to the experimental values and also no significant differences have been observed between models.[71] We used the GIAO method[78,79] as

(70) Haeberlen, U. High resolution NMR in solids. Selective averaging. In *Advances in Magnetic Resonance*; Waugh, J. S. , Ed.; Academic Press: New-York, 1965; Vol. 1.
(71) Solans-Monfort, X.; Filhol, J. S.; Copéret, C.; Eisenstein, O. *New J. Chem.* **2006**, *30*, 842–850.
(72) Bloechl, P. E. *Phys. Rev. B: Condens. Matter.* **1994**, *50*, 17953–17979.
(73) Kresse, G.; Joubert, D. *Phys. Rev. B: Condens. Matter.* **1999**, *59*, 1758–1775.
(74) Kresse, G.; Furthmüller, J. *Phys. Rev. B: Condens. Matter.* **1996**, *54*, 11169–11186.
(75) Kresse, G.; Furthmüller, J. *Comput. Mater. Sci.* **1996**, *6*, 15–50.
(76) Perdew, J. P.; Burke, K.; Ernzerhof, M. *Phys. Rev. Lett.* **1996**, *77*, 3865–3868.
(77) MacDonald, A. H. *Phys. Rev. B: Condens. Matter.* **1978**, *18*, 5897–5899.
(78) Ditchfield, R. *J. Chem. Phys.* **1972**, *56*, 5688–5691.

implemented in Gaussian03 package.[80] The NMR calculations are obtained by carrying out B3PW91 single point calculations on the previously optimized periodic structure (it has been shown previously that PBE and B3PW91 functionals give similar results).[71] In those calculations, Re, Mo W, Ta, and Si atoms are represented with the quasirelativistic effective core pseudopotentials (RECP) of the Stuttgart group and the associated basis sets augmented with a polarization function.[81–84] The remaining O, N, C, and H atoms were represented with Kutzelnigg's IGLO-II basis sets.[85,86] This methodology has been reported to perform with reasonable accuracy for organometallic complexes both for chemical shifts[45] and $^1J_{CH}$ coupling constants.[86,87]

The output of the DFT NMR chemical shift calculations, performed with Gaussian03, is the absolute shielding tensor σ. The chemical shift δ is given by $\delta = -(\sigma - \sigma^{ref})$, where σ^{ref} is the nuclear shielding of the reference system. To compare experiment and calculated results, the shielding must be converted to the chemical shift using a reference shielding, tetramethylsilane (TMS) in this study. One can calculate σ^{ref} of TMS (σ^{TMS}) but this might introduce unnecessary errors (see below). Thus as an alternative approach, the calculated shielding σ_{iso}^{calc} is plotted against the experimental shifts δ_{iso}^{exp} and a linear regression is performed, imposing a slope of unity according to the formula given above. The shielding σ_{iso}^{calc} is then converted to chemical shift δ_{iso}^{calc} using the reference σ_{iso}^{TMS} obtained from the regression. For ^{13}C data, a fit of the calculated cluster_1 data σ_{iso}^{calc} against the experimental values δ_{iso}^{exp} yielded an intercept of 179.7 ppm for the reference shielding σ_{iso}^{TMS} and had a rmsd of 7.9 ppm. A fit of the calculated cluster_2 data σ_{iso}^{calc} against the experimental values δ_{iso}^{exp} yielded an intercept of 179.9 ppm for the reference shielding σ_{iso}^{TMS} and had a rmsd of 7.7 ppm. A fit of the calculated data of both cluster_1 and 2 σ_{iso}^{calc} against the experimental values δ_{iso}^{exp} yielded an intercept of 179.8 ppm for the reference shielding σ_{iso}^{TMS} and had a rmsd of 11.0 ppm. When the correlation was carried out without restriction on the slope (the fitted value of which became 1.04 for cluster_1, cluster_2 and, both cluster_1 and 2 together), the rmsd errors are 7.3, 6.9 and 10.0 ppm for cluster_1, cluster_2, and cluster_1 and 2, respectively. The intercept σ_{iso}^{TMS} also changed to 183.6, 184.1, and 183.4 ppm for cluster_1, cluster_2 and, cluster_1 and 2, respectively. Note that using the DFT calculated shielding value for TMS, $\sigma_{iso}^{calc(TMS)}$ of 186.8 ppm (value closed to the value reported in the literature)[88] to convert calculated shielding σ_{iso}^{calc} into calculated chemical shift δ_{iso}^{exp}, the rmsd errors are found to be larger at 10.6 and 10.4 ppm for cluster_1 and 2, respectively. With regards to these data and in keeping with the expression $\delta = -(\sigma - \sigma^{ref})$ for relating the shift to the shielding, obtaining the reference shift σ_{iso}^{TMS} by constraining the slope of unity for cluster_1 and cluster_2, is the preferred approach used here.

The principal components of the chemical shift tensor are given by δ_{11}, δ_{22}, and δ_{33} and obtained by diagonalization of the full 3 × 3 chemical shielding tensor matrix. Isotropic δ_{iso}^{calc}, anisotropic chemical shift δ_{aniso}^{cal} and asymmetry parameters η^{calc} are obtained from the chemical shift tensor using the Haeberlen convention[70] as mentioned in the text. The drawings of the chemical shift tensors (Figures 10 and S19) have been performed with a ray-tracing computer software application (POV-Ray, Persistance Of Vision Raytracer Pty. Ltd., version 3.6 available at www.pov-ray.org).

3. Results

3.1. Residual Dipolar Coupling Constants. Motional averaging can be observed through the CH dipolar tensors. Separated local field (SLF) spectroscopy[89] correlates the carbon-13 isotropic chemical shifts with the CH dipolar interactions in a two-dimensional experiment. We have used the dipolar shift correlation experiment (dipshift),[51,90,91] integrating DUMBO[58,59] type homonuclear decoupling and recorded over ω_1 during t_1 sampled over a single rotor period.[60–62] This experiment is suitable to measure directly bonded ^{13}C−^{1}H pairs where dipolar couplings are large and rotational sidebands are intense.[92–94] At low MAS frequency, a two-dimension Fourier transform yields a 2D spectrum correlating the chemical shift spinning sideband patterns (in F_2) with the symmetrized heteronuclear dipolar spinning sideband spectra (in F_1). Fitting these heteronuclear dipolar spinning sidebands leads to the ^{13}C−^{1}H dipolar couplings constant b_{CH} as defined previously in eq 1.

To validate the protocol, spectra from L-alanine were recorded (Figure S2), and we obtained values of $<b_{CH}^{exp}> = -7.0 \pm 0.3$ and -23.9 ± 0.5 kHz for the C_β and C_α carbons (Table 1), respectively, in good agreement with the literature.[95]

Dipolar spectra measured in this way for the alkylidene carbons [M]=***C***H and methylene carbons [M]***C***H$_2$ are shown in Figures 2 and 3 for [**ReR**] and *syn*-[**MoR**] and in Figures S3−S6 for [**TaR**], [**WR**], [**MoNPh$_2$**], and [**MoPy**]. The dipolar spectra of the methylene [Re]***C***H$_2$, *syn*-alkylidene *syn*-[Re]=***C***H and *anti*-alkylidene *anti*-[Re]=***C***H[14] of [**ReR**] are shown in Figure 2 (in blue) along with the simulated spectra (in red) obtained with the best fit heteronuclear dipolar coupling constants $<b_{CH}^{exp}>$ of -12.5 ± 3.0, -11.0 ± 4.1, and -10.9 ± 4.9 kHz (Table 1), respectively. The measured values are significantly lower than the expected values $<b_{CH}^{exp}>$ of −21.3, −22.8, and −21.5 kHz (green spectra in Figure 2), based on the calculated bond distances (Table S1) and eq 1, for a rigid solid.[65] They are therefore a clear indication of fast limit dynamics of the complex. For *syn*-[**MoR**] (Figure 3), experimental dipolar coupling constants $<b_{CH}^{exp}>$ of -19.5 ± 1.6 and -19.7 ± 2.7 kHz (Table 1) were obtained for [Mo]***C***H$_2$ and *syn*-[Mo]=***C***H, values which are closer to the ones expected for a rigid system, i.e., −22.4 and −21.6 kHz, respectively.

Similarly, the CH dipolar coupling constants of the alkylidene [M]=***C***H and methylene [M]***C***H$_2$ carbons of all the other complexes (Chart 1) were also determined and are reported in

(79) Lee, A. M.; Handy, N. C.; Colwell, S. M. *J. Chem. Phys.* **1995**, *103*, 10095–10109.
(80) Pople, J. A. et al. *Gaussian 03*, Version D; Gaussian Inc.: Wallingford, CT, 2004.
(81) Andrae, D.; Haeussermann, U.; Dolg, M.; Stoll, H.; Preuss, H. *Theor. Chim. Acta* **1990**, *77*, 123–141.
(82) Bergner, A.; Dolg, M.; Kuechle, W.; Stoll, H.; Preuss, H. *Mol. Phys.* **1993**, *80*, 1431–1441.
(83) Ehlers, A. W.; Boehme, M.; Dapprich, S.; Gobbi, A.; Hoellwarth, A.; Jonas, V.; Koehler, K. F.; Stegmann, R.; Veldkamp, A. *Chem. Phys. Lett.* **1993**, *208*, 111–114.
(84) Hoellwarth, A.; Boehme, M.; Dapprich, S.; Ehlers, A. W.; Gobbi, A.; Jonas, V.; Koehler, K. F.; Stegmann, R.; Veldkamp, A. *Chem. Phys. Lett.* **1993**, *208*, 237–240.
(85) Kutzelnigg, W.; Fleischer, U.; Schindler, M. In *NMR Basic Principles and Progress*; Diehl, P., Fluck, E., Gunter, H. , Kosfeld, R., Seelig, J. , Eds.; Springer-Verlag: Berlin, 1990; Vol. 23, pp 165–263..
(86) Solans-Monfort, X.; Eisenstein, O. *Polyhedron* **2006**, *25*, 339–348.
(87) Bolton, P. D.; Clot, E.; Adams, N.; Dubberley, S. R.; Cowley, A. R.; Mountford, P. *Organometallics* **2006**, *25*, 2806–2825.
(88) Jameson, A. K.; Jameson, J. C. *Chem. Phys. Lett.* **1987**, *134*, 461–466.
(89) Hester, R. K.; Ackerman, J. L.; Neff, B. L.; Waugh, J. S. *Phys. Rev. Lett.* **1976**, *36*, 1081–1083.
(90) Munowitz, M. G.; Griffin, R. G. *J. Chem. Phys.* **1982**, *76*, 2848–2858.
(91) Munowitz, M.; Aue, W. P.; Griffin, R. G. *J. Chem. Phys.* **1982**, *77*, 1686–1689.
(92) Griffiths, J. M.; Griffin, R. G. *Anal. Chim. Acta* **1993**, *283*, 1081–1101.
(93) Huster, D.; Xiao, L.; Hong, M. *Biochemistry* **2001**, *40*, 7662–7674.
(94) Franks, W. T.; Zhou, D. H.; Wylie, B. J.; Money, B. G.; Graesser, D. T.; Frericks, H. L.; Sahota, G.; Rienstra, C. M. *J. Am. Chem. Soc.* **2005**, *127*, 12291–12305.
(95) Lorieau, J.; McDermott, A. E. *Magn. Reson. Chem.* **2006**, *44*, 334–347.

Table 1. Best-Fit Dipolar Coupling Constants and Order Parameter ($<S_z>^{RDC}$) Obtained for Alanine and Different Carbon Sites (Alkylidene [M]=***C***H and Methylene [M]***C***H_2) of Surface Organometallic Complexes

	NMR[a]		
site	δ_{iso}^{exp} (ppm)	$<b_{CH}^{exp}>$ (kHz)	$<S_z>^{RDC}$[b]
	Alanine		
CH$_\alpha$	19	-23.9 ± 0.5	1.03 ± 0.03
CH$_{3\beta}$	51	-7.0 ± 0.3	0.31 ± 0.02
	[ReR]		
syn-[Re](=***CH****t*Bu)	247	-11.0 ± 4.1	0.51 ± 0.19
anti-[Re](=***CH****t*Bu)	257	-10.9 ± 4.9	0.48 ± 0.22
syn-[Re](***CH***$_2$*t*Bu)	44	-12.5 ± 3.0	0.56 ± 0.14
anti-[Re](***CH***$_2$*t*Bu)	*c*		
	[TaR]		
[Ta](=***CH****t*Bu)	245	-11.6 ± 5.1	0.55 ± 0.25
[Ta](***CH***$_2$*t*Bu)	96	-11.4 ± 3.8	0.52 ± 0.18
	[MoR]		
syn-[Mo](=***CH****t*Bu)	279	-19.7 ± 2.7	0.91 ± 0.13
anti-[Mo](=***CH****t*Bu)		*d*	
syn-[Mo](***CH***$_2$*t*Bu)	56	-19.5 ± 1.6	0.87 ± 0.08
anti-[Mo](***CH***$_2$*t*Bu)		*d*	
	[WR]		
syn-[W](=***CH****t*Bu)	255	-13.4 ± 1.4	0.62 ± 0.07
anti-[W](=***CH****t*Bu)		*d*	
syn-[W](***CH***$_2$*t*Bu)	60	-14.4 ± 1.4	0.64 ± 0.07
anti-[W](***CH***$_2$*t*Bu)		*d*	
	[MoNPh$_2$]		
syn-[Mo](=***CH****t*Bu)	288	-17.3 ± 3.1	0.80 ± 0.18
anti-[Mo](=***CH****t*Bu)		*d*	
	[MoPy]		
syn-[Mo](=***CH****t*Bu)	285	-19.5 ± 4.2	0.91 ± 0.20
anti-[Mo](=***CH****t*Bu)		*d*	

[a] Experimental proton carbon distance determined from dipshift spectroscopy by fitting the observed dipolar spectra. Estimated errors are estimated on the basis of the noise level. [b] Order parameters are measured from the experimental determined dipolar coupling constant where the static limit dipolar coupling constant is determined by DFT calculations. (see Table S1). Estimated errors are calculated while taking account the estimated errors in experimental dipolar coupling constant. Reference 66 was used for the DFT calculations of alanine. [c] No specific signal has been detected for the *C*H_2 carbon of the *anti* isomer. The signal for this carbon, which should appear around 47 ppm (according to model compound), is probably buried under the broad *C*H_2 carbon of the *syn* isomer at 44 ppm.[14] [d] The isomerization *syn*/*anti* of the alkylidene [M]=CH could not be observed experimentally.

Table 1. In all cases, the obtained dipolar coupling constants are lower than the predicted static value of –22.5 kHz from eq 1, showing that the complexes undergo fast limit motional averging on the NMR timescales.

3.2. Residual Chemical Shift Anisotropy. 3.2.1. Measurement of Chemical Shift Anisotropy. Chemical shift anisotropy (CSA)[96] reflects the orientation dependence of the chemical shift with respect to the external magnetic field B_0 due to the anisotropic electron distribution. The chemical shift interaction is described by a second rank tensor δ with the principal components (δ_{11}, δ_{22}, δ_{33}). In solution, the chemical shift interaction is averaged by molecular tumbling to the isotropic chemical shift δ_{iso} defined as:

$$\delta_{iso} = \frac{1}{3}(\delta_{11} + \delta_{22} + \delta_{33}) \quad (2)$$

In crystalline samples, CSA gives rise to characteristic line shapes (CSA powder patterns) reflecting its tensor nature and from which the principal components may be obtained directly.[30,67] Using the Haeberlen convention,[70] the width of the spectra is related to the chemical shift anisotropy δ_{aniso}, which is a measure of how sensitive the interaction is to the orientation:

$$\delta_{aniso} = \delta_{11} - \delta_{iso} \quad (3)$$

The deviation from axial symmetry is defined by the asymmetry parameter η as:

$$\eta = \frac{\delta_{22} - \delta_{33}}{\delta_{11} - \delta_{iso}} \quad (4)$$

where the absolute value varies from 0 to 1. The CSA interaction provides a very sensitive probe for molecular dynamics since motions in the submillisecond time scale will partially or fully averaged out the chemical shift anisotropy.[38] Thus comparison of the average values $<\delta_{aniso}>$ and $<\eta>$ with the static values yields information on the dynamics.

Experimentally, the CSA can be determined in the slow spinning regime when the magic angle frequency ω_r is less than the CSA and spinning side bands are observed.[97] The sideband patterns consist of a series of resonances centered on the isotropic chemical shift and spaced by ω_r. The intensity distribution of this spectrum is characteristic of the CSA tensor and used to extract the CSA parameters mention above.[67] In our case, the carbon sites of interest in the molecules have different isotropic chemical shift values (the δ_{iso} are in the range of 50–100 and 250–300 ppm for methylene [M]***C***H_2 and alkylidene [M]=***C***H carbons, respectively)[98] and the spinning sideband patterns of both carbons in the slow spinning regime do not overlap, and thus simple ^{13}C CP spectrum was used to obtain the CSA parameters.

The ^{13}C CSA principal components of the carbons directly bonded to the metal of all complexes (Chart 1) have been obtained by fitting the spinning sideband patterns in the slow spinning regimes as described above. At MAS frequency of 12.5 kHz, the ^{13}C CP MAS spectrum of Re ([**ReR**]) (Figure 4a, black) (recorded with a CP contact time of 1 ms) presents three resonances at isotropic chemical shift δ_{iso}^{exp} of 247, 44, and 30 ppm (Tables 2 and 4) already assigned to the alkylidene [Re](=***C***H*t*Bu), methylene [Re](***C***H_2*t*Bu), and methyl (*t*Bu).[12,14] The unprotonated alkylidyne carbon [Re](≡***C****t*Bu) is observed at an isotropic chemical shift of 292 ppm (Table 3) using a longer contact time of 10 ms (Figure 5a, black).[12,14]

Reducing the spinning rate to 4 kHz, the ^{13}C CP MAS spectrum of [**ReR**] reveals spinning sideband patterns for the alkylidene [Re](=***C***H*t*Bu) (Figure 4b, blue) and the alkylidyne [Re](≡***C****t*Bu) (Figure 5b, blue) resonances at an isotropic shift δ_{iso}^{exp} of 247 (Figure 4a, black) and 292 ppm (Figure 5a, black), respectively. The experimental chemical shift anisotropies of the alkylidene and alkylidyne ligands, fitted from the sideband intensities,[67] are $<\delta_{aniso}^{exp}> = 125 \pm 6$ and -140 ± 5 ppm, respectively (Tables 2 and 3). The best fit simulated spectra[63] are shown in Figures 4c and 5c (red) to illustrate the quality of the agreement. Note that it was not possible to observe spinning side bands for the methylene carbons [Re](***C***H_2*t*Bu) at $\delta_{iso}^{exp} =$

(96) Grant, D. M. Chemical shift tensors. In *Encyclopedia of Nuclear Magnetic Resonance*; Grant, D. M. , Harris, R. K., Eds.; Wiley: Chichester, 1996; Vol. 2, pp 1298–1321..

(97) Orendt, A. M. Chemical shift tensor measurement, in solids. In *Encyclopedia of Nuclear Magnetic Resonance*; Grant, D. M., Harris, R. K., Eds.; Wiley: Chichester, 1996; Vol. 2, pp 1282–1297..

(98) Schrock, R. R. *Chem. Rev.* **2002**, *102*, 145.

Table 2. Experimental and Calculated Carbon Chemical Shielding Tensor Elements (δ_{ii}), Anisotropic Parameters (δ_{aniso}, η) and Order Parameter ($<S_z>^{CSA}$) of the Alkylidene Fragments [M]=***C***H[a]

complexes	δ_{iso}	δ_{11}	δ_{22}	δ_{33}	δ_{aniso}	η	$<S_z>^{CSA}$[b]
***syn*-[ReR]**[c]	**247**	**372**	**239**	**130**	**125 ± 6**	**0.87 ± 0.04**	
syn-ReR-C1	259	565	118	95	306	0.08	0.41±0.05
syn-ReR-C2	260	567	119	95	307	0.08	
***anti*-[ReR]**	**257**			not determined[d]			
anti-ReR-C1	273	603	166	51	330	0.35	
anti-ReR-C2	274	605	167	51	331	0.35	
[TaR]	**245**	**394**	**205**	**136**	**149 ± 8**	**0.46 ± 0.20**	
TaR-C1	219	501	158	−3	282	0.57	0.53±0.08
TaR-C2	220	502	160	−3	282	0.58	
***syn*-[MoR]**	**279**	**574**	**156**	**107**	**295 ± 9**	**0.16 ± 0.06**	
syn-MoR-C1	286	647	121	89	361	0.09	0.82±0.04
syn-MoR-C2	286	648	122	89	362	0.09	
***anti*-[MoR]**				not observed[e]			
anti-MoR-C1	316	713	159	75	397	0.21	
anti-MoR-C2	317	715	160	76	398	0.21	
***syn*-[WR]**	**255**	**429**	**219**	**117**	**174 ± 4**	**0.70 ± 0.08**	
syn-WR-C1	241	547	112	63	306	0.16	0.57±0.04
syn-WR-C2	241	547	113	63	302	0.17	
***anti*-[WR]**				not observed[e]			
anti-WR-C1	266	603	129	67	337	0.18	
anti-WR-C2	267	604	130	68	336	0.18	
***syn*-[MoNPh$_2$]**	**288**	**494**	**225**	**145**	**206 ± 2**	**0.40 ± 0.05**	
syn-MoNPh$_2$-C1	301	673	123	107	372	0.04	0.55±0.02
syn-MoNPh$_2$-C2	302	681	133	114	372	0.05	
***anti*-[MoNPh$_2$]**	**302**			not determined[d]			
anti-MoNPh$_2$-C1	320	727	155	79	407	0.19	
anti-MoNPh$_2$-C2	323	730	157	81	407	0.19	
***syn*-[MoNPy]**	**285**	**603**	**181**	**71**	**318 ± 3**	**0.34 ± 0.06**	
syn-MoNPy-C1	301	684	126	93	383	0.09	0.83±0.03
syn-MoNPy-C2	301	685	126	93	384	0.08	
***anti*-[MoNPy]**				not observed[e]			
anti-MoNPy-C1	334	754	164	84	420	0.19	
anti-MoNPy-C2	334	754	164	85	420	0.19	

[a] δ_{ii} are the principal components of the carbon CS tensor such that $|\delta_{11} - \delta_{iso}| > |\delta_{33} - \delta_{iso}| > |\delta_{22} - \delta_{iso}|$. Carbon CS tensor parameters are $\delta_{iso} = (\delta_{11} + \delta_{22} + \delta_{33})/3$, $\delta_{aniso} = \delta_{11} - \delta_{iso}$ and $\eta = (\delta_{22} - \delta_{33})/(\delta_{11} - \delta_{iso})$. Experimental carbon chemical shifts are referenced to liquid TMS at 0 ppm. Experimental carbon CS tensor were determined by fitting the observed spinning side bands at $\nu_R = 4$ kHz. Experimental values are provided in bold face. Models for calculated data are with the full ligands, the silica being replaced by -OSi(OH)$_3$ for cluster_1 (C1) and by -OSi(OSi(OH)$_3$)$_3$ for cluster_2 (C2), respectively. The shieldings were converted to chemical shift using a reference value of 179.7 and 179.8 ppm obtained from a constrained linear regression of cluster_1 and cluster_2, respectively. [b] Order parameters are measured from the experimental determined anisotropy where the static limit dipolar coupling constant is determined by DFT calculations. Estimated errors are calculated using the estimated errors in experimental δ_{aniso} and the standard deviation for experimental vs calculated chemical shift. [c] The followings carbon chemical shift tensor anisotropy and asymmetry were obtained for the [Re]=***C***H resonance: 132 ± 7 ppm and 0.87 ± 13 while fitting the spinning sideband patterns on the spectrum recorded at 10 ms contact time (Figure 3b). [d] The intensity of the spinning sidebands of the alkylidene [M]=***C***H*t*Bu resonance of the *anti* isomers is too low to determine the CSA tensor. [e] The isomerization *syn*/*anti* of the alkylidene [M]=***C***H*t*Bu could not be observed experimentally.

Table 3. Experimental and Calculated Carbon Chemical Shielding Tensor Elements (δ_{ii}), Anisotropic Parameters (δ_{aniso}, η), and Order Parameter ($<S_z>^{CSA}$) of the Alkylidyne Ligands [M]≡***C*** in [**ReR**][a]

complexes	δ_{iso}	δ_{11}	δ_{22}	δ_{33}	δ_{aniso}	η	$<S_z>^{CSA}$[b]
***syn*-[ReR]**	**292**	**421**	**302**	**152**	**−140 ± 5**	**0.86 ± 0.14**	
syn-ReR-C1	309	484	406	36	−273	0.29	0.51±0.05
syn-ReR-C2	308	483	406	36	−272	0.28	
***anti*-[ReR]**	**302**			not determined[c]			
anti-ReR-C1	318	487	414	53	−265	0.28	
anti-ReR-C2	318	487	415	52	−266	0.27	

[a] δ_{ii} are the principal components of the carbon CS tensor such that $|\delta_{11} - \delta_{iso}| > |\delta_{33} - \delta_{iso}| > |\delta_{22} - \delta_{iso}|$. Carbon CS tensor parameters are $\delta_{iso} = (\delta_{11} + \delta_{22} + \delta_{33})/3$, $\delta_{aniso} = \delta_{11} - \delta_{iso}$ and $\eta = (\delta_{22} - \delta_{33})/(\delta_{11} - \delta_{iso})$. Experimental carbon chemical shifts are referenced to liquid TMS at 0 ppm. Experimental carbon CS tensor were determined by fitting the observed spinning side bands at $\nu_R = 4$ kHz. Experimental values are provided in bold face. Models for calculated data are with the full ligands, the silica being replaced by -OSi(OH)$_3$ for cluster_1 (C1) and by -OSi(OSi(OH)$_3$)$_3$ for cluster_2 (C2), respectively. The shieldings were converted to chemical shift using a reference value of 179.7 and 179.8 ppm obtained from a constrained linear regression of cluster_1 and cluster_2, respectively. [b] Order parameters are measured from the experimental determined anisotropy where the static limit dipolar coupling constant is determined by DFT calculations. Estimated errors are calculated using the estimated errors in experimental δ_{aniso} and the standard deviation for experimental vs calculated chemical shift. [c] The intensity of the spinning sidebands of the alkylidyne [Re]≡***C***t*Bu resonance of the *anti* isomers is too low to determined the CSA tensor.

44 ppm (Figure S7), showing that the CSA is probably around 5 – 10 ppm due to fast motional averaging.

Similarly, we have determined the ^{13}C CSA principal components of α-carbons of all other complexes (Chart 1) and their corresponding best fits are given in Figures 6, 7, S7−S13 and Tables 2–4. The obtained anisotropies for metal–carbon multiple bonds (alkylidene [M](=***C***H*t*Bu) and alkylidyne [Re](≡***C***t*Bu)) are large ranging from 125 ppm for [Re](=***C***H*t*Bu) in [**ReR**] to 318 ppm for [Mo](=***C***H*t*Bu) in [**MoPy**] (Tables 2 and 3). Those values are in good agreement

Table 4. Experimental and Calculated Carbon Chemical Shielding Tensor Elements (δ_{ii}), Anisotropic Parameters (δ_{aniso}, η) and Order Parameter ($<S_z>^{CSA}$) of the Methylene Fragments [M]***C***H_2[a]

complexes	δ_{iso}	δ_{11}	δ_{22}	δ_{33}	δ_{aniso}	η	$<S_z>^{CSA}$[b]
***syn*-[Re]**	**44**			not determined[c]			
syn-ReR-C1	46	65	47	25	21	0.87	
syn-ReR-C2	46	65	47	25	21	0.87	
anti-[Re]	*d*			not determined[c]			
anti-ReR-C1	47	73	47	21	26	0.97	
anti-ReR-C2	47	72	47	22	25	1	
[TaR]	**96**	**121**	**93**	**74**	**25 ± 1**	**0.68 ± 0.05**	
TaR-C1 C^1H_2[e]	56	109	48	12	53	0.68	
TaR-C1 C^2H_2[e]	72	114	77	24	48	0.78	0.47 ± 0.15
TaR-C2 C^1H_2[e]	57	109	49	13	52	0.69	
TaR-C2 C^2H_2[e]	72	115	77	24	48	0.79	
***syn*-[Mo]**	**56**	**76**	**52**	**40**	**20 ± 1**	**0.61 ± 0.05**	
syn-MoR-C1	50	98	51	1	49	0.96	
syn-MoR-C2	50	99	51	1	49	0.97	0.41 ± 0.05
anti-[Mo]				not observed[f]			
anti MoR-C1	65	106	51	38	41	0.32	
anti-MoR-C2	65	107	51	38	42	0.31	
***syn*-[W]**	**60**	**80**	**60**	**40**	**20 ± 2**	**1.0 ± 0.3**	
syn-WR-C1	48	91	51	2	46	0.82	
syn-WR-C2	45	85	50	0	45	0.77	0.44 ± 0.18
anti-[W]				not observed[f]			
anti-WR-C1	57	95	48	28	38	0.53	
anti-WR-C2	57	95	49	28	38	0.56	

[a] δ_{ii} are the principal components of the carbon CS tensor such that $|\delta_{11} - \delta_{iso}| > |\delta_{33} - \delta_{iso}| > |\delta_{22} - \delta_{iso}|$. Carbon CS tensor parameters are $\delta_{iso} = (\delta_{11} + \delta_{22} + \delta_{33})/3$, $\delta_{aniso} = \delta_{11} - \delta_{iso}$ and $\eta = (\delta_{22} - \delta_{33})/(\delta_{11} - \delta_{iso})$. Experimental carbon chemical shifts are referenced to liquid TMS at 0 ppm. Experimental carbon CS tensor were determined by fitting the observed spinning side bands at $\nu_R = 1.5$ kHz. Experimental values are provided in bold face. Models for calculated data are with the full ligands, the silica being replaced by -OSi(OH)$_3$ for cluster_1 (C1) and by -OSi(OSi(OH)$_3$)$_3$ for cluster_2 (C2), respectively. The shieldings were converted to chemical shift using a reference value of 179.7 and 179.8 ppm obtained from a constrained linear regression of cluster_1 and cluster_2, respectively. [b] Order parameters are measured from the experimental determined anisotropy where the static limit dipolar coupling constant is determined by DFT calculations. Estimated errors are calculated using the estimated errors in experimental δ_{aniso} and the standard deviation for experimental vs calculated chemical shift. [c] The lack of the spinning sidebands of the methylene [Re]***C***H_2*t*Bu prevents the determination of the CSA tensor. [d] No specific signal has been detected for the *C*H_2 carbon of the *anti* isomer. The signal for this carbon, which should appear around 41 ppm (according to model compound), is probably buried under the broad *C*H_2 carbon of the *syn* isomer at 44 ppm.[14] [e] The two CH_2 carbons of TaR-C*x* (x = 1 or 2) are found inequivalent in the DFT calculations. [f] The isomerization *syn*/*anti* of the alkylidene [M]=*C*H*t*Bu could not be observed experimentally.

with values (Table S2) previously measured for π bonded systems such as double bonded (one π bond: C=C,[99–102] C=O,[103] and C=Cr[104]) and triple bonded carbons (two π bonds: C≡C).[100,105,106] Note that we have also determined the ^{13}C CSA of both methylene [Ta]***C***H_2 and alkylidene [Ta]=***C***H carbons of [**TaR**] as the function of temperature (see Figures S14, S15 and Table S3). A slight increase in CSA of the ^{13}C CSA is observed while decreasing the temperature (for example the ^{13}C CSA of [Ta]=***C***H increased from 136 ppm at 313 K to 168 ppm at 193 K (Table S3)). This notably confirms the presence of motion in this sample.

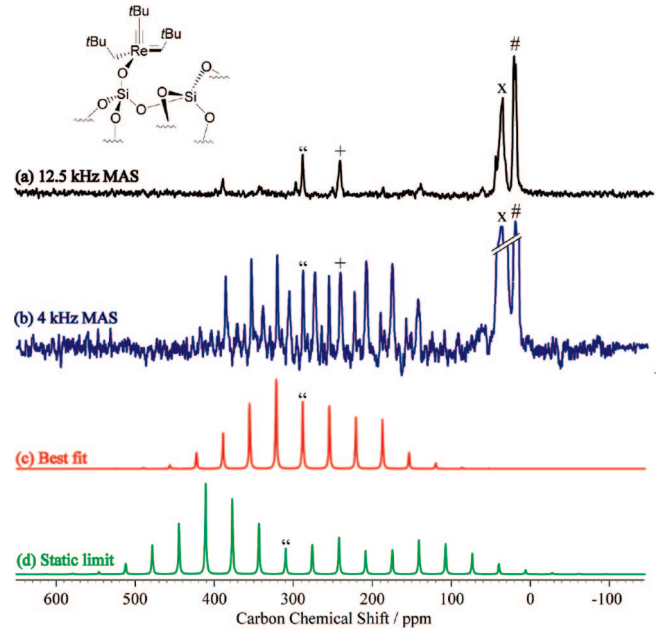

Figure 5. NMR spectra of *syn*-[(≡SiO)Re(≡*C*t*Bu)(=*CH*t*Bu)(*CH_2*t*Bu)] ([**ReR**]). (a) Black: ^{13}C CP MAS spectrum recorded at ν_R = 12.5 kHz with 15360 transients. The contact time for CP was set to 10 ms. (b) Blue: ^{13}C CP MAS spectrum recorded at ν_R = 4 kHz with 3000 transients. The contact time for CP was set to 10 ms. (c) Red: best-fit simulated spinning side bands of the alkylidyne carbon [Re](**C***t*Bu) (δ_{iso}^{exp} = 292 ppm, $<\delta_{aniso}^{exp}>$ = –140 ± 5 ppm, $<\eta^{exp}>$ = 0.86 ± 0.14). (d) Green: simulation of the spinning side bands of the alkylidyne carbon of the models ***syn*-ReR-C1** (δ_{iso}^{calc} = 309 ppm, δ_{aniso}^{calc} = −273 ppm, η^{calc} = 0.29). Labels “, +, ×, and # show the isotropic resonances of the alkylidyne [Re]**C***t*Bu, alkylidene [Re]=***C***H (*syn* and *anti*), methylene [Re]***C***H_2 and the ***C***H_3 (not ^{13}C-labeled) resonance, respectively. All experimental details are as described previously in Figure 4.

So far, we have determined experimentally the carbon-13 CSA tensor at room temperature, which is, in principle, the averaged CSA tensor. Access to dynamics is not available since the static limit value δ_{aniso}^{calc} is not directly measurable in any simple way. Here we propose to use static limit values obtained from accurate DFT calculations (which do not take account the dynamics) to obtain δ_{aniso}^{calc}. Therefore in the following, we have calculated the principal components of the chemical shift tensors, validated the calculations by comparison between experimental and calculated isotropic chemical shifts δ_{iso}^{exp} and δ_{iso}^{calc}, and then used the calculated anisotropic chemical shifts δ_{aniso}^{calc} as the static limit values.

3.2.2. Chemical Shift Calculations. 3.2.2.1. Calculated Isotropic Chemical Shifts. We compare the calculated and experimental carbon ^{13}C isotropic chemical shifts, which should not be significantly affected by dynamics. There is an overall very good agreement between calculated δ_{iso}^{calc} and experimental δ_{iso}^{exp} carbon ^{13}C isotropic chemical shifts of all complexes (Chart

(99) Zilm, W. K.; Beeler, A. J.; Grant, D. M.; Miehl, J. *J. Am. Chem. Soc.* **1980**, *102*, 6672–6676.
(100) Zilm, W. K.; Grant, D. M. *J. Am. Chem. Soc.* **1981**, *103*, 2913–2922.
(101) Orendt, A. M.; Facelli, J. C.; Beeler, A. J.; Reuter, K.; Horton, W. J.; Cutts, P.; Grant, D. M.; Michl, J. *J. Am. Chem. Soc.* **1988**, *110*, 3386–3392.
(102) Huang, Y.; Gilson, F. R. D.; Butler, S. I. *J. Chem. Soc., Dalton Trans.* **1992**, 2881–2883.
(103) Wei, Y.; Lee, D.-K.; Ramamoorthy, A. *J. Am. Chem. Soc.* **2001**, *123*, 6118–6126.
(104) Havlin, R.; McMahon, M.; Srinivasan, R.; Le, H. B.; Oldfield, E. *J. Phys. Chem. A* **1997**, *101*, 8908–8913.
(105) Beeler, A. J.; Orendt, A. M.; Grant, D. M.; Cutts, P. W.; Michl, J.; Zilm, K. W.; Downing, J. W.; Facelli, J. C.; Schindler, M. S.; Kutzelnigg, W. *J. Am. Chem. Soc.* **1984**, *106*, 7672–7676.
(106) Harris, K. J.; Bernard, G. M.; McDonald, C.; McDonald, R.; Ferguson, M. J.; Wasylishen, R. E. *Inorg. Chem.* **2006**, *45*, 2461–2473.

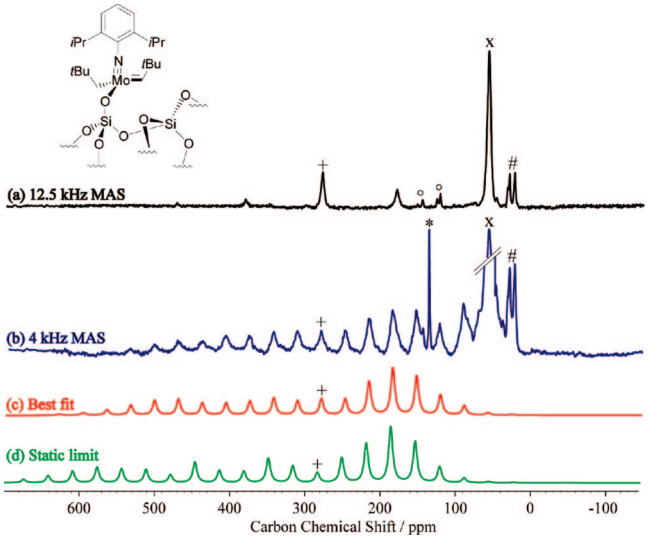

Figure 6. NMR spectra of *syn*-[(≡SiO)Mo(≡NAr)(=*CH*t*Bu)(*CH_2*t*Bu)] ([**MoR**]). (a) Black: ^{13}C CP MAS spectrum recorded at ν_R = 12.5 kHz with 40000 transients. (b) Blue: ^{13}C CP MAS spectrum recorded at ν_R = 4 kHz with 35000 transients. (c) Red: best-fit simulated spinning side bands of the alkylidene carbon *syn*-[Mo](=***C***H*t*Bu) (δ_{iso}^{exp} = 279 ppm, $<\delta_{aniso}^{exp}>$ = 295 ± 9 ppm, $<\eta^{exp}>$ = 0.16 ± 0.06). (d) Green: simulation of the spinning side bands of the alkylidene carbon of the models ***syn*-MoR-C1** (δ_{iso}^{calc} = 286 ppm, δ_{aniso}^{calc} = 361 ppm, η^{calc} = 0.09). Labels +, ×, °, and # show the isotropic resonances of the alkylidene *syn*-[Mo]=***C***H, methylene [Mo]***C***H_2, the aromatics (not ^{13}C-labeled), and the ***C***H_3 (not ^{13}C-labeled) resonance, respectively. Asterisk (*) indicates small decomposition of the product during acquisition (<2% by integration). All experimental details are as described previously in Figure 4.

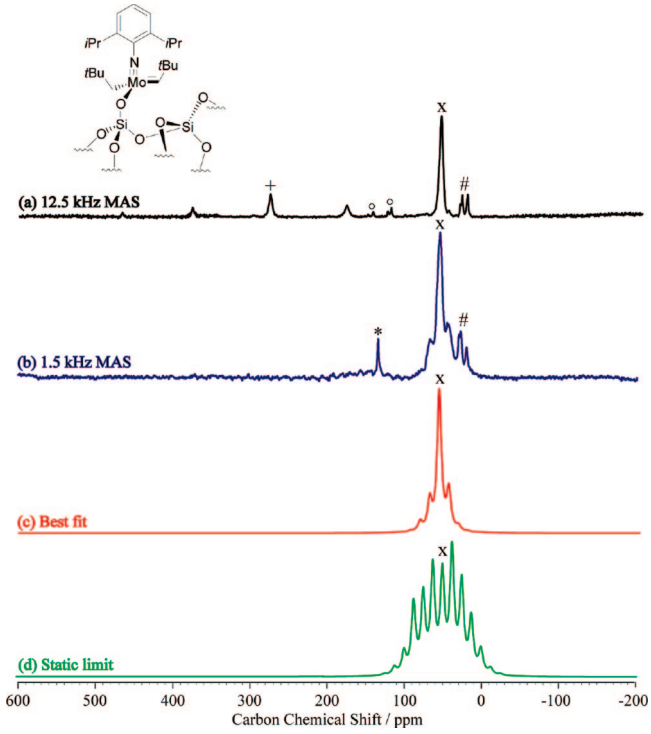

Figure 7. NMR spectra of *syn*-[(≡SiO)Mo(≡NAr)(=*CH*t*Bu)(*CH_2*t*Bu)] ([**MoR**]). (a) Black: ^{13}C CP MAS spectrum recorded at ν_R = 12.5 kHz with 40000 transients. (b) Blue: ^{13}C CP MAS spectrum recorded at ν_R = 1.5 kHz with 20480 transients. The contact time for CP was 2 ms. (c) Red: best-fit simulated spinning side bands of the methylene carbon [Mo](−***C***H_2*t*Bu) (δ_{iso}^{exp} = 56 ppm, $<\delta_{aniso}^{exp}>$ = 20 ± 1 ppm, $<\eta^{exp}>$ = 0.61 ± 0.05). (d) Green: simulation of the spinning side bands of the methylene carbon of the models ***syn*-MoR-C1** (δ_{iso}^{exp} = 50 ppm, δ_{aniso}^{calc} = 49 ppm, η^{calc} = 0.96). Labels +, ×, °, and # show the isotropic resonances of the alkylidene [Mo]=***C***H, methylene [Mo]***C***H_2, the aromatics (not ^{13}C-labeled), and the ***C***H_3 (not ^{13}C-labeled) resonance, respectively. Asterisk (*) indicates small decomposition of the product during acquisition (<2% by integration). All experimental details are as described previously in Figure 4.

1), as illustrated by the correlation plot in Figure 8 and Table S4. The standard deviation σ (rmsd) between the calculated and experimental isotropic chemical shifts are found to be 7.9 and 7.7 ppm for cluster_1 and cluster_2, respectively. This shows that the size of the silicate cluster has negligible effect on chemical shielding as illustrated earlier.[71] The largest deviation is observed for the α-carbon bonded directly to the metal center but even here the agreement is still good (see below). These calculated values are given in Tables 2–4 in comparison with the experimental data for the α-carbons in all the complexes considered here (Chart 1). Considering only the isotropic carbon chemical shift of α-carbons, the correlation coefficient is 0.993 with a slope of 0.91, an intercept of 18.1 ppm and a rmsd of 16.5 ppm (or 5% of the whole experimental range of 309 ppm) for cluster_1, and the correlation coefficient is 0.993 with a slope of 0.90, an intercept of 17.9 ppm and a rmsd of 16.7 ppm (or 5% of the whole experimental range of 309 ppm) for cluster_2, respectively. The largest deviations are 26 and 32 ppm (ca 10–33%) for the alkylidene [Ta]=***C***H and methylene [Ta]−***C***H_2 in the tantalum complex (Tables 2 and 4). It has been shown that the calculations of the NMR responses do not agree so well with the experimental values when strong agostic interactions are present.[86] This can be due to the fact that thermal effects and anharmonicity have been neglected which are more important for weaker CH bond.[46] This accounts for the poorer results for Ta=CHR, which has a strong α-agostic interaction as evidenced by the very low $^1J_{CH}$ and the wide Ta−C_{ene}−C angle (see Table 5 and Table S1) but seems also to occur for Ta−CH_2.

These data clearly validate that the isotropic chemical shift (eq 2), i.e., the trace of the shielding tensor, is sufficiently well described by DFT to be confident that the calculated NMR tensors are also a reliable description of the intrinsic static CSA tensors (δ_{11}, δ_{22}, δ_{33}). We propose then to compare them with the experimental data to evaluate the dynamics of the grafted complexes.

3.2.2.2. Static Limit Anisotropic Chemical Shifts. The calculated anisotropies δ_{aniso}^{calc} are obtained from the calculated principal components of the chemical shift (δ_{11}, δ_{22}, δ_{33}) using eq 3, and the resulting data are shown in Tables 2–4 for the all the α-carbons bonded to metals. The corresponding predicted static limit spectra were simulated for all the complexes and are shown in green below the experimental best fit. First, one should note that the experimental $<\delta_{aniso}^{exp}>$ and calculated δ_{aniso}^{calc} anisotropies have the same sign as found in previous work in π-bonded systems.[99–106] Moreover the calculated anisotropies δ_{aniso}^{calc} are always larger than the experimental anisotropies $<\delta_{aniso}^{exp}>$ (Tables 2–4). In the alkylidene moieties [M]=***C***H, the biggest difference between calculations and experimental data is obtained for [**TaR**] with $\delta_{aniso}^{calc} - <\delta_{aniso}^{exp}>$ = 181 ppm and the smallest for [**MoPy**] with $\delta_{aniso}^{calc} <\delta_{aniso}^{exp}>$ = 63 ppm, and this would indicate a much larger dynamics for [**TaR**] than [**MoPy**] (vide infra for further details). These differences are an indication of molecular motion, which partially averages the CSA tensors and therefore reduces the width of the anisotropy δ_{aniso} (vide infra).[32,38,107]

(107) Pines, A.; Gibby, M. G.; Waugh, J. S. *J. Chem. Phys.* **1973**, *59*, 569–590.

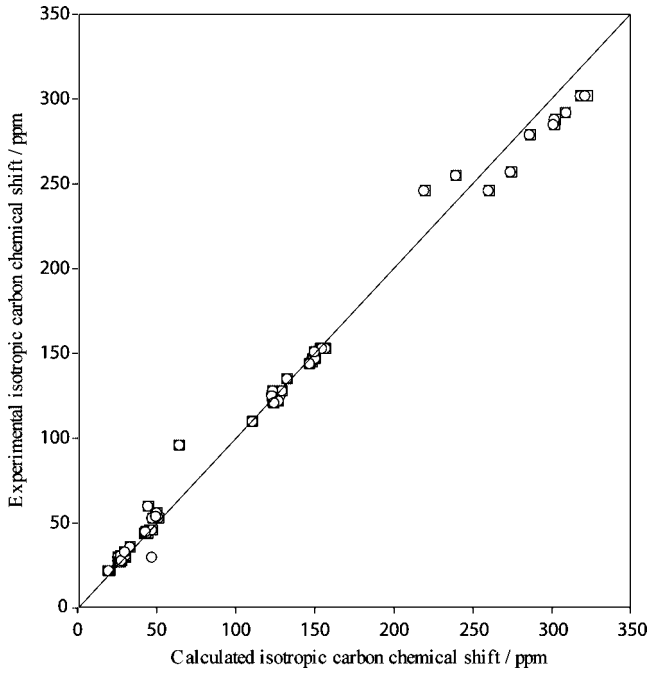

Figure 8. Combined plot of the calculated δ_{iso}^{calc} versus the experimental δ_{iso}^{exp} values for all isotropic ^{13}C chemical shift of silica-supported complexes. Circles and squares are for cluster_1 and cluster_2, respectively, used for the DFT calculations. Rmsd values of 7.9 and 7.7 ppm for cluster_1 and cluster_2 were obtained, respectively. The shieldings were converted to chemical shift using a reference value of 179.7 and 179.8 ppm obtained from a constrained linear regression of cluster_1 and cluster_2, respectively.

Table 5. Calculated M−C_{ene}−H Bond Angle, and Calculated and Experimental $^1J_{CH}$ Coupling Constants[a]

complexes	calculated M−C_{ene}−H bond angle	$^1J_{CH}$ (Hz)	
		calculated	experimental
***syn*-ReR**	103.5	107	109[13]
***anti*-ReR**	121.8	141	159[13]
TaR	94.5	94	80[16]
***syn*-MoR**	98.8	105	110[9]
***anti*-MoR**	116.0	128	*b*
***syn*-WR**	99.9	101	*c*
***anti*-WR**	116.0	126	*b*,*c*
***syn*-MoNPh$_2$**	99.5	107	107[9]
***anti*-MoNPh$_2$**	117.0	131	*b*
***syn*-MoPy**	98.9	106	109[9]
***anti*-MoPy**	121.9	140	*b*

[a] The calculated bond angle is given from the cristoballite ($C_{(110)}$) model and the calculated $^1J_{CH}$ coupling constant from cluster_1. For computational reason, we have not calculated the $^1J_{CH}$ coupling constant from cluster_2 as we have shown recently that the size of the cluster has virtually no effect on $^1J_{CH}$.[71] The experimental $^1J_{CH}$ coupling constants have been obtained previously as given.[9,13,16] [b] The isomerization *syn*/*anti* of the alkylidene [M]=CH could not be observed experimentally. [c] Not determined.

4. Discussion

4.1. Differential Molecular Dynamics. Two different dynamic probes, i.e., dipolar coupling constants and ^{13}C CSA tensors of various silica-supported complexes [(≡SiO)M(ER)(=CH*t*Bu)(R′)] (Chart 1) have been determined both experimentally and computationally. Motional averaging is determined by comparison of the measured residual dipolar and CSA tensors with the calculated static dipolar and CSA tensors. Visual inspection of Figures 2−7 and S3−S13 shows clearly that different degrees of motion are observed for the different sites and complexes.

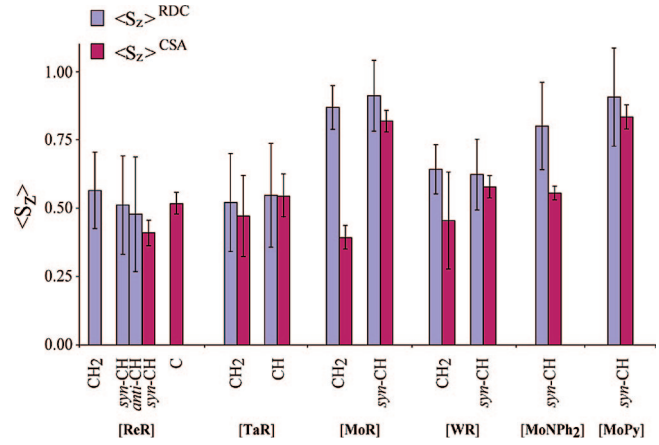

Figure 9. Plots of the dipolar coupling order parameter $<S_z>^{RDC}$ (blue) and chemical shift anisotropy order parameter $<S_z>^{CSA}$ (red) versus carbon sites for silica-supported complexes [(≡SiO)Re(≡C*t*Bu)(=CH*t*Bu)(CH_2*t*Bu)] ([**ReR**]), [(≡SiO)Ta(=CH*t*Bu)(CH_2*t*Bu)$_2$] ([**TaR**]), *syn*-[(≡SiO)Mo(≡NAr)(=CH*t*Bu)(CH_2*t*Bu)] (***syn*-[MoR]**), *syn*-[(≡SiO)W(≡NAr)(=CH*t*Bu)(CH_2*t*Bu)] (***syn*-[WR]**), *syn*-[(≡SiO)Mo(≡NAr)(=CH*t*Bu)(NPh_2)] (***syn*-[MoNPh$_2$]**), and *syn*-[(≡SiO)Mo(≡NAr)(=CH*t*Bu)(NC_4H_4)] (***syn*-[MoPy]**). The [**ReR**] complex has two different dipolar coupling order parameters $<S_z>^{RDC}$ for the CH moieties coming from the *syn* (left) and *anti* (right) isomers. The low CSA of the methylene [Re]−***C***H_2 carbon prevents its measurement. The intensity of the spinning sidebands of the *anti*-alkylidene [Re]=***C***H resonance CH is too low to determined the CSA tensor and then $<S_z>^{CSA}$.

The dynamics can be quantified through an order parameter[38,52–55] that we defined as $<S_z>^{RDC}$ for residual dipolar couplings:

$$<S_z>^{RDC} = \frac{\langle b_{CH}^{exp} \rangle}{b_{CH}^{calc}} \quad (5)$$

which ranges from 0 (for fully isotropic mobility) to 1 (for rigid molecule) for a given carbon where $<b_{CH}^{exp}>$ and b_{CH}^{calc} are the experimental averaged and calculated static dipolar coupling constants (obtained for a rigid system, see Table S1),[65] respectively. Dipolar order parameters $<S_z>^{RDC}$ are found to be 0.56 ± 0.14, 0.51 ± 0.19, and 0.48 ± 0.22 for the methylene [Re]***C***H_2, *syn*-alkylidene [Re]=***C***H and *anti*-alkylidene [Re]=***C***H moieties for [**ReR**] (Table 1), respectively. Similar dipolar order parameters are obtained for the methylene [Ta]***C***H_2 (0.52 ± 0.18) and alkylidene [Ta]=***C***H (0.55 ± 0.25) carbons for [**TaR**], respectively (Table 1). Slightly larger order parameters $<S_z>^{RDC}$ of 0.62 ± 0.07 and 0.64 ± 0.07 are obtained for the *syn* alkylidene [W]=***C***H and methylene carbons [W]***C***H_2 of [**WR**], respectively. In contrast the alkylidene moieties for [**MoR**], [**MoNPh$_2$**], and [**MoPy**] (Chart 1) have substantially larger dipolar order parameter $<S_z>^{RDC}$ of 0.91 ± 0.13, 0.80 ± 0.18, and 0.91 ± 0.20, respectively. Figure 9 plots the dipolar order parameters $<S_z>^{RDC}$ for all the carbons studied here.

In addition to the dipolar order parameters $<S_z>^{RDC}$, we have also shown that the experimental reduced anisotropies $<\delta_{aniso}^{exp}>$ are always smaller than the calculated static δ_{aniso}^{calc}, which is a complementary probe for motional averaging on the millisecond time scale.[38] The quantification of the motion can also be performed by defining a CSA order parameter $<S_z>^{CSA}$ as follows:

$$<S_z>^{CSA} = \frac{\langle \delta_{aniso}^{exp} \rangle}{\delta_{aniso}^{calc}} \quad (6)$$

Figure 9 also plots the CSA order parameters $<S_z>^{CSA}$ as a function of the carbon moieties for all the silica-supported

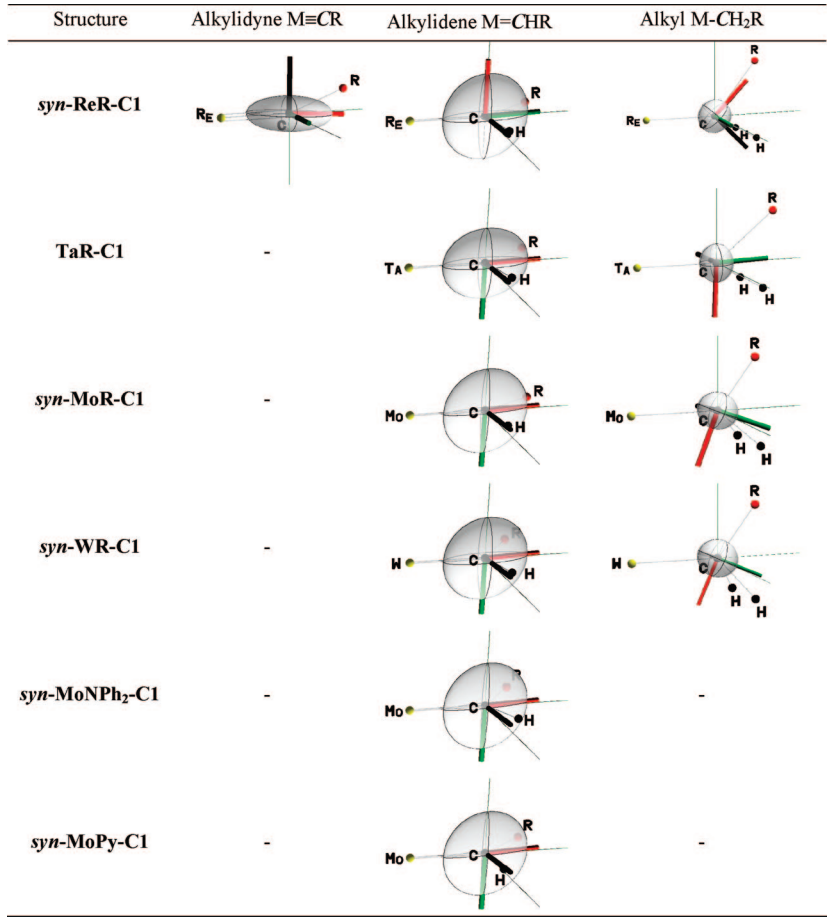

Figure 10. POV-Ray rendering of the shielding tensor's orientations of the alkylidene M=*C*HR, methylene M−*C*H$_2$R and alkylidyne Re≡*C*R (R = *t*Bu) moieties of all complexes. The tensor orientations and structural parameters have been generated from the DFT calculations of the *syn* calculated structure using cluster_*x* (*x* = 1 or 2). Only cluster_1 is given above. The black, green, and red colors are used for σ_{11}, σ_{22}, and σ_{33} tensor principal components, respectively.

complexes. We remark that for the majority of sites, the order parameters obtained from CSA are the same as those obtained from RDC, and the agreement is especially correct for alkylidene carbons [M]=*C*H. First, these results validate the definition of $<S_z>^{CSA}$ and second ratify further the use of computational chemistry to determine static limit CSA tensors, which could not be obtained experimentally by low-temperature measurements as discussed above on [**TaR**] (see Figures S14 and S15 and Table S3). Moreover, the CSA has the enormous advantage to be much easier to measure reliably than the heteronuclear dipolar coupling.

Therefore, *it is shown that the different complexes in the series considered here undergo significantly different dynamic behaviors*. In the first place, it is of great interest to prove that there is a substantial and quantitative difference in dynamics from one system to another as reported through the order parameters (Figure 9). They do not however yield a detailed picture of the exact geometry of motion occurring, which is out of the scope of the current work. This will require further measurements using for example ^{2}H NMR which would require extensive synthetic chemistry (see Chart 1) and will be published elsewhere in due course. Nevertheless, we can provide here a first simple qualitative discussion of the possible averaging scheme that the data does constrain. For example, one possibility to interpret the dipolar order parameters $<S_z>^{RDC}$ in Figure 9 is that roughly speaking we find that the complexes bearing the bulky diisopropylphenylimido ligand [M]≡NAr, i.e., [**MoR**], [**WR**], [**MoNPh$_2$**], and [**MoPy**] (Chart 1) have larger order parameters than [**ReR**] and [**TaR**], which have less bulky ligands. With the imido ligand, however, the tungsten complex [**WR**] appears more mobile despite its bulky ligand. This would indicate that molecular motion on the silica surface is hindered by bulky and/or aromatic ligands. However, another way to interpret the order parameters is to note that the Mo complexes (2nd row in the periodic table) are rigid, while all the third row 5d metals (Ta, W, Re) show significant greater mobility (with the bulky W ligand having slightly more rigidity).

Importantly, we note that even in the most mobile systems, we never find a null order parameter ($<S_z> = 0$). This is clear evidence that *the motion in these systems is neither isotropic nor jumps between equivalent tetrahedral sites*.[30,32] Furthermore, and perhaps unexpectedly, our data clearly shows that the motion is *not free uniaxial rotations or jumps between more than three sites*, for which an axially symmetric averaged tensor ($<\eta> = 0$) would be expected.[30] This speaks against motions via simple rotation around the Si−O and/or O−M bonds, and against mobility similar to what has aleady been observed for silica-supported Rh species.[108]

On the contrary, all the tensors we observe have $<\eta>$ different from 0. The closest tensor to axial symmetry ($<\eta> = 0.16 \pm 0.06$) is obtained for the largest CSA order parameter

(108) Dufour, P.; Scott, S. L.; Santini, C. C.; Lefebvre, F.; Basset, J.-M. *Inorg. Chem.* **1994**, *33*, 2509–2517.

(0.82 ± 0.02) of the alkylidene carbon [Mo]=*C*H in [**MoR**] and all the other residual CSA tensors have $<\eta>$ larger than 0.34. Thus, we propose that *the ligand motions are either jump motions between 2 sites*, for example docking of the aromatic group with the surface using van der Waals interactions, or (more probably) *restricted librational motions*. Molecular dynamics simulations are under way to understand the quantitative variations in η.

4.2. Chemical Shift Tensors as Probes of Agosticity. The orientations of the principal axes of the shielding tensor in the molecular frame are also obtained from the DFT calculations; the shielding tensors are shown graphically in Figure 10 and superimposed on the molecular fragments. For ***syn*-ReR-Cx**, the alkylidyne carbon, i.e., a metal–carbon triple bond [M]≡*C*, has a shielding tensor orientation and shape similar to that of acetylene[100,105] (see Figure S19 and Table S2) with δ_{33} along the M-C σ-bond, and δ_{11} and δ_{22} being of smaller and identical magnitudes (Figure 10 and Table 3). For the *syn*- and *anti*-alkylidene carbon, i.e., a metal–carbon double bond [Re]=*C*, the shielding tensor is oriented similarly to ethene:[99,100] with δ_{33} perpendicular to the double bond, δ_{11} and δ_{22} in the plane of the alkylidene, and δ_{22} being aligned along the M=C bond. Note however that δ_{33} and δ_{22} are very similar in magnitude for the *syn* complexes, in contrast to ethene, where $\delta_{33} << \delta_{22}$ (see below for further comments, Figure S19 and Table S2).[99,100] For the alkyl, the tensor of the methylene carbons of the metal-alkyl, [Re]-*C*H_2, has no particular preferred orientation, yielding an almost isotropic tensor (Figure 10).[109,110]

For the other systems **TaR-Cx**, ***syn*-MoR-Cx**, ***syn*-WR-Cx**, ***syn*-MoNPh$_2$-Cx**, and ***syn*-MoPy-Cx**, the shape of the shielding tensors is generally similar to that of ***syn*-ReR-Cx**, but *their orientation is along the M-C σ-bond, as in the case of the alkylidyne carbon of **syn-ReR-Cx***. The degree of anisotropy of the tensor around the M-C σ-bond, as reported by η, depends on the metal, and the trend is as follows: Ta ≫ W > Mo ≈ Re. Interestingly, this trend is correlated with the strength of the agostic interaction in the M−C_{ene}−H moiety, as evidenced by the calculated M−C_{ene}−H bond angles (Tables 5 and S1) as well as by the calculated and experimental $^1J_{CH}$ values,[9,13,16] which are well-known reporters of agosticity (Table 5).[111–115] The distortion of the M−C_{ene}−H bond in an agostic interaction corresponds to a change of hybridation of the alkylidene carbon from sp^2 toward sp (typically evidenced by the low $^1J_{CH}$ value) and here we see that it translates *into a characteristic distortion of the chemical shift tensor, which tends toward that of an alkylidyne as the agostic interaction or the s character on carbon increases*. We note finally that, as expected, the alkylidene carbon of *anti* complexes, which do not present any agostic interactions (vide supra, Tables 5 and S1), has a CSA tensor oriented similarly to ethene (Figure S20).

5. Conclusion

Differential dynamics properties are observed through residual ^{1}H−^{13}C dipolar couplings and ^{13}C chemical shift anisotropies in a series of alkylidene-based surface organometallic catalysts [(≡SiO)M(ER)(=CH*t*Bu)(R′)] (Chart 1) using solid-state NMR spectroscopy. While a canonical geometry could be used to detect residual dipolar couplings, time-averaged anisotropies requires the knowledge of the static limit chemical shift tensor, which could only be obtained by low-temperature measurements. However, an excellent agreement is observed between the experimental and DFT calculated isotropic ^{13}C chemical shifts showing that the chemical shift tensors are accuratly determined. Thus, we used calculated tensors for the static limit values and found differences between experimental and calculated chemical shift tensors which strongly support molecular motion, and are cross validated by the dipolar measurements.

Quantification of the dynamics by determination of dipolar and chemical shift order parameters yields values ranging from 0.5 for mobile complexes [**ReR**] and [**TaR**] to 0.9 for rigid systems [**MoR**], [**MoNPh$_2$**], and [**MoPy**]. These dynamic behaviors are tentatively related to the presence of bulky ligands and/or to the 4d or 5d nature of the metals. Qualitative analysis of the data reveals that the motion is not isotropic and could be either jumps between two sites or restricted librational motions. Moreover, distortion of the calculated ^{13}C chemical shift tensor of alkylidene toward that of an alkylidyne is related to the increasing strength of the agostic interaction. Further measurements, for example using deuterium, or including low-temperature measurements when technically feasible, would obviously be of great interest in the future to validate these mechanisms and to further explore the dynamics and energetics revealed here.

Finally, the data shown here illustrate that differential dynamics is present in surface complexes. These complexes also have different reactivity, stability, and selectivity.[16,18,22–25] This leads to the exciting possibility that the dynamics may play a role in determining chemical activity, with the perspective in the future of establishing dynamics−activity relationships for these types of materials (where dynamics has not so far been considered to play a key role in reactivity).

Acknowledgment. F.B. is grateful to the French Ministry of Education, Research and Technology (MENRT) for a graduate fellowship. X.S.-M. thanks the CNRS for a postdoctoral fellowship, followed by a associate researcher position. He also thanks the Spanish Ministerio de Educación y Ciencia for a 5-year Ramón y Cajal associate researcher position. We are grateful to Dr. Bénédicte Eléna for making fitting sidebands routines available to us, to Gwendal Kervern for POV-Ray rendering, and to Antoine Loquet for assistance with variable-temperature calibration. The IDRIS (061744) and CINES (lsd2217) French national computing centers as well as CESCA are acknowledged for a generous donation of computational time. Insightful discussions with Profs. Clare P. Grey and Rob W. Schurko are gratefully acknowledged. We are indebted to the CNRS, ANR (ANR JC05_46372), ESCPE Lyon, ENS Lyon and the National Science Foundation (CHE-0138495) for financial supports. Most of the spectra reported here were acquired at the Rhône-Alpes Large Scale Facility for High Field NMR Spectroscopy (www.ralf-nmr.fr).

(109) Zilm, K. W.; Beeler, A. J.; Grant, D. M.; Michl, J.; Chou, T. C.; Allred, E. L. *J. Am. Chem. Soc.* **1981**, *103*, 2119–2120.
(110) Facelli, J. C.; Orendt, A. M.; Beeler, A. J.; Solum, M. S.; Depke, G.; Malsch, K. D.; Downing, J. W.; Murthy, P. S.; Grant, D. M.; Michl, J. *J. Am. Chem. Soc.* **1985**, *107*, 6749–6754.
(111) Brookhart, M.; Green, M. L. H. *J. Organomet. Chem.* **1983**, *250*, 395–408.
(112) Brookhart, M.; Green, M. L. H.; Wong, L. L. *Prog. Inorg. Chem.* **1988**, *36*, 1–124.
(113) Clot, E.; Eisenstein, O. Agostic interaction from a computational perspective: one name, many interpretations. In *Structure and Bonding, Computational Inorganic Chemistry*; Kaltzoyannis, N., McGrady, J. E., Eds.; Spinger-Verlag: Heidelberg, 2004; Vol. 113, pp 1–36..
(114) Brookhart, M.; Green, M. L. H.; Parkin, G. *Proc. Natl. Acad. Sci. U.S.A.* **2007**, *104*, 6908–6914.
(115) Fung, B. M.; Khitrin, A. K.; Ermolaev, K. *J. Magn. Reson.* **2000**, *142*, 97–101.

Supporting Information Available: Discussion and full computational details of the DFT calculated structures, pulse program for dipshift using DUMBO-1 (Figure S1), CH dipolar spectra of alanine (Figure S2), [(≡SiO)Ta(=CH*t*Bu)(CH_2*t*Bu)$_2$] (Figure S3), [(≡SiO)W(≡NAr)(=CH*t*Bu)(CH_2*t*Bu)] (Figure S4), [(≡SiO)Mo(≡NAr)(=CH*t*Bu)(NPh_2)] (Figure S5), [(≡SiO)Mo(≡NAr)(=CH*t*Bu)(NC_4H_4)] (Figure S6), NMR spectra of [(≡SiO)Re(≡C*t*Bu)(=CH*t*Bu)(CH_2*t*Bu)] (Figure S7), [(≡SiO)Ta(=CH*t*Bu)(CH_2*t*Bu)$_2$] (Figure S8−S9), [(≡SiO)W(≡NAr)(=CH*t*Bu)(CH_2*t*Bu)] (Figure S10−S11), (≡SiO)Mo(≡NAr)(=CH*t*Bu)(NPh_2)] (Figure S12), [(≡SiO)Mo(≡NAr)(=CH*t*Bu)(NC_4H_4)] (Figure S13), variable-temperature NMR spectra of [(≡SiO)Ta(=CH*t*Bu)(CH_2*t*Bu)$_2$] (Figure S14), plot of the chemical shift anisotropy of [(≡SiO)Ta(=CH*t*Bu)(CH_2*t*Bu)$_2$] versus temperature (Figure S15), full list of authors for ref 80, periodic optimized structures (Figure S16), finite SiO shell structures for chemical shift calculations (Figure S17), DOS curves (Figure S18), calculated tensor's orientation of CS tensor of acetylene, ethene, and ethane (Figure S19) and all *anti* complexes (Figure S20), and selected calculated bond distances and angles (Table S1), experimental and calculated NMR tensor of acetylene, ethene, and ethane (Table S2), variable-temperature experimental NMR tensor data of [(≡SiO)Ta(=CH*t*Bu)(CH_2*t*Bu)$_2$] (Table S3), isotropic experimental and calculated carbon chemical shift (Table S4), and list of Cartesian coordinates of all complexes. This material is available free of charge via the Internet at http://pubs.acs.org.

JA077749V